NON-ISOMETRIC NEUROMUSCULAR ELECTRICAL STIMULATION VIA NON-MODEL BASED NONLINEAR CONTROL METHODS

By

KEITH STEGATH

A THESIS PRESENTED TO THE GRADUATE SCHOOL
OF THE UNIVERSITY OF FLORIDA IN PARTIAL FULFILLMENT
OF THE REQUIREMENTS FOR THE DEGREE OF
MASTER OF SCIENCE

UNIVERSITY OF FLORIDA

2007

To my wife whose support enabled me to return to college, my father whose integrity never faltered, and my mother whose short life was filled with love and compassion.

ACKNOWLEDGMENTS

My gratitude goes to the numerous people who allowed me the freedom to improve existing skills and guidance in developing new ones.

TABLE OF CONTENTS

page

ACKNOWLEDGMENTS iv

LIST OF TABLES vii

LIST OF FIGURES viii

ABSTRACT x

CHAPTER

1 INTRODUCTION 1

2 EXTREMUM SEEKING CONTROL SCHEME 8

2.1 Control Objective 10
2.2 Extremum Generation 10
2.3 Experimental Results 13
2.3.1 Experimental Testbed 13
2.3.2 Experimental Setup 15
2.3.3 Optimal Voltage Seeking Results 15
2.3.4 Optimal Frequency Seeking Results 18
2.4 Discussion 22
2.5 Concluding Remarks 22

3 NONLINEAR CONTROL SCHEME 24

3.1 Robust Integral Sign of the Error 24
3.2 Muscle Activation and Limb Model 26
3.3 Control Development 28
3.4 Experimental Results 31
3.4.1 Experimental Setup 32
3.4.2 Regulation Results 32
3.4.3 Tracking Results 34
3.5 Discussion 37
3.6 Concluding Remarks 40

4 CONCLUSIONS AND RECOMMENDATIONS 41

APPENDIX

ELECTRICAL DESIGN AND INTERFACING 43

A.1 Circuit Design for 100 μsec Wide Pulse 43
A.2 Circuit Description 43
A.2.1 High Voltage Power Op-Amp PA866EU 45
A.2.2 Voltage to Frequency Conversion - VFC32 47
A.2.3 Transistors 2N3565 48
A.2.4 Voltage Regulator 7805 49
A.2.5 Circuit Behavior 49
A.3 Interfacing the 100 μsec Wide Pulse PCB to the Computer 49
A.4 Circuit Design for Multiples of 25 μsec Wide Pulse 50
A.4.1 Circuit Description 50
A.5 Isometric Attachment 53

REFERENCES 55

BIOGRAPHICAL SKETCH 59

LIST OF TABLES

Table		page
2–1	Determining whether to change the upper or lower bound.	13
2–2	Knee-joint angle controlled by voltage	17
2–3	RMS error and steady-state error for Brent's Method using VM	19
2–4	Knee-joint angle controlled by frequency	21
2–5	RMS error and steady-state error for Brent's Method using FM	22
3–1	RMS and steady-state error for RISE regulation experiments	36
3–2	RMS and steady-state error for RISE tracking experiments	39
A–1	Input voltages to circuit	45
A–2	Parts list for stimulator circuit	48
A–3	Digital inputs to the circuit	52
A–4	The effect of the relay on the corresponding pulse width	52
A–5	Parts list for pulse width controller	53

LIST OF FIGURES

Figure page

1–1 Leg angle generated with a constant voltage for one second with a 100 μs wide pulse delived at 20 Hz. Stimulation voltages were 25, 30, 35, and 40 volts. . . . 3

1–2 Leg angle generated with a constant frequency for one second with a 100 μs wide pulse delivered at 40 volts. The stimulation frequencies were 1, 5, 10, and 20 Hz. . . . 4

2–1 Leg curl and extension machine after modifications. . . . 14

2–2 Online computed voltage (long dashed), desired leg angle (short dashed), and actual leg angle (solid). . . . 17

2–3 Brent's Method overshooting the desired angle before converging towards the solution using VM. . . . 18

2–4 Online computed frequency (bold solid), desired leg angle (short dashed), and actual leg angle (solid). . . . 20

2–5 Brent's Method converging on the solution using FM. . . . 21

3–1 Knee-joint angle defined by q. . . . 27

3–2 Typical muscle excursion of the test subjects used for the regulation and tracking experiments. . . . 33

3–3 Regulation of knee joint angle using the RISE controller. . . . 34

3–4 Regulation voltage using the RISE controller. . . . 35

3–5 Regulation error of knee joint angle (desired angle minus actual angle). . . . 35

3–6 Desired tracking profile extended to 20 seconds. . . . 37

3–7 Knee joint tracking using the RISE controller. . . . 38

3–8 Tracking voltage using the RISE controller. . . . 38

3–9 Tracking error of knee joint angle (desired angle minus actual angle). . . . 39

A–1 Schematic of circuitry used to deliver the computed stimulation pulse train. . . . 44

A–2 PCB layout of circuitry used to deliver the computed pulse train. 45
A–3 Circuit board used to generate and amplify a 100 μsec pulse. 46
A–4 Shape of stimulation pulse. 47
A–5 Circuit for adjusting the pulse width with steps of 25 μ sec. 51
A–6 Circuit diagram for S-beam load cell. 54

Abstract of Thesis Presented to the Graduate School
of the University of Florida in Partial Fulfillment of the
Requirements for the Degree of Master of Science

NON-ISOMETRIC NEUROMUSCULAR ELECTRICAL STIMULATION VIA NON-MODEL BASED NONLINEAR CONTROL METHODS

By

Keith Stegath

December 2007

Chair: Warren E. Dixon
Major: Mechanical Engineering

For people afflicted with neuromuscular disorders such as stroke or spinal cord injuries, there has been limited success by engineers and biological researchers to artificially control the afflicted person's muscles with neuromuscular electrical stimulation (NMES). NMES is the application of an electrical current via internal or external electrodes which results in a muscle contraction. NMES is currently prescribed to treat muscle atrophy and impaired motor control associated with orthopedic and neurological damage, circulatory impairments, joint motion dysfunction, postural disorders, swelling and inflammatory reactions, slow-to-heal wounds and ulcers, and incontinence. The development of NMES as a neuroprosthesis has grown rapidly because of the potential improvement in the activities of daily living for individuals with movement disorders such as stroke and spinal cord injuries.

Researchers have mainly focused on two methods to deliver the electrical signal to the muscle, direct nerve stimulation with electrodes inserted through the skin or implanted under the skin, and surface stimulation where adhesive-backed electrodes are placed on the skin. While each method has its advantages and

disadvantages, a barrier to both methods that limits further application of NMES is that an unknown mapping exists between the stimulation parameters (e.g., voltage, frequency, and pulse width) to muscle force production. In one situation, different stimulation parameters will yield significantly different contraction forces, while in another situation an infinite combination of the parameters can yield the same contraction force. In addition to the variability in stimulation parameters, the muscle contraction force is difficult to predict due to a variety of uncertainties related to muscle physiology (e.g., architecture, temperature, and pH) and the ability to consistently deliver the stimulation (e.g., electrode placement, resistance variations due to subcutaneous fat). The practical limitations imposed for some NMES applications due to the uncertain relationship between stimulation parameters and the force produced by the muscle provided the motivation to explore methods that can compensate for these uncertainties.

CHAPTER 1
INTRODUCTION

Neuromuscular electrical stimulation (NMES) is the application of a potential field across a muscle via internally or externally placed electrodes in order to produce a desired muscle contraction. NMES is a prescribed treatment for a number of neurological dysfunctions. Because of the potential for improvements in daily activities by people with movement disorders such as stroke and spinal cord injuries, the development of NMES as a neuroprosthesis has grown rapidly [1]. However, the application and growth of NMES technologies have been stymied by several technical challenges related to the design of an automatic stimulation strategy. Specifically, due to a variety of uncertainties in muscle physiology (e.g., temperature, pH, and architecture), predicting the exact contraction force exerted by the muscle is difficult. One cause of this difficulty is that there is an unknown mapping between the generated muscle force and stimulation parameters. There are additional problems with delivering consistent stimulation energy to the muscle due to electrode placement, percentage of subcutaneous body fat, muscle fatigue, as well as overall body hydration. There are also time delays between the delivery of the stimulation signal and the contraction of the muscle.

Given the uncertainties in the structure of the muscle model and the parametric uncertainty for specific muscles, some investigators have explored various linear PID-based pure feedback methods [2–6]. Typically, these approaches have only been empirically investigated and no analytical stability analysis has been developed that provides an indication of the performance, robustness or stability of these control methods. Some recent studies [7] point to evidence that suggests linear control methods do not yield acceptable performance. The development of a stability

analysis for previous PID-based NMES controllers has been evasive because of the fact that the governing equations for muscle contraction/limb motion are nonlinear with unstructured uncertainties. Some efforts have focused on analytical control development for linear controllers [5, 8, 9]; however, the governing equations are typically linearized to accommodate a gain scheduling or linear optimal controller approach.

Motivated by the lack of control development for PID-based feedback methods, significant research efforts have focused on the use of neural network-based controllers [10–18]. Nonlinear neural network methods provided a framework that allowed the performance, robustness, and stability of the developed NMES controllers to be investigated without linearization assumptions. However, all previous neural network-based NMES controllers are limited to a uniformly ultimately bounded result because of the inevitable residual nonlinear function approximation error. Additionally, neural networks may exhibit performance degradation during the transient phase while the estimates update.

The major barrier for further application of NMES is that an unknown mapping exists between the stimulation parameters (e.g., amplitude, frequency, pulse shape, pulse width, pulse train) and the muscle force production. This issue occurs for both isometric and non-isometric muscle contraction. In addition to an infinite combination of stimulation parameters that yield equivalent muscle contraction forces, modulating different stimulation parameters yields different contraction force profiles (Fig. 1–1 and 1–2). These figures are representative of a non-isometric NMES experimental comparison performed with a pulse train of one-second applied to the quadriceps. Fig. 1–1 shows the knee-joint angle generated with different voltages using a stimulation frequency of 20 Hz with a 100 μs wide pulse, while Fig. 1–2 measures the knee-joint angle generated with constant voltage and pulse width (40 volts and 100 μs respectively) but varying the frequency.

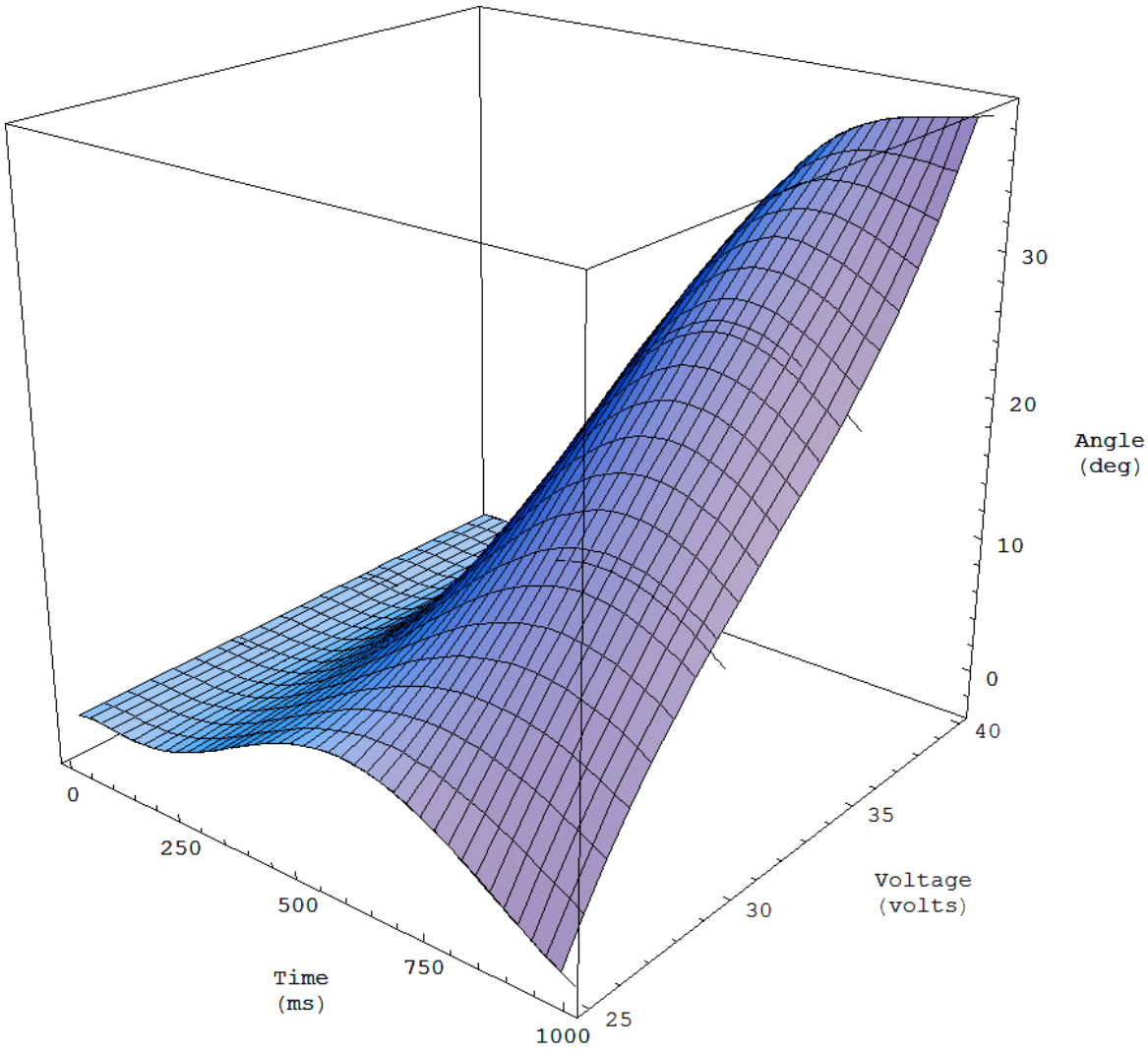

Figure 1–1: Leg angle generated with a constant voltage for one second with a 100 μs wide pulse delived at 20 Hz. Stimulation voltages were 25, 30, 35, and 40 volts.

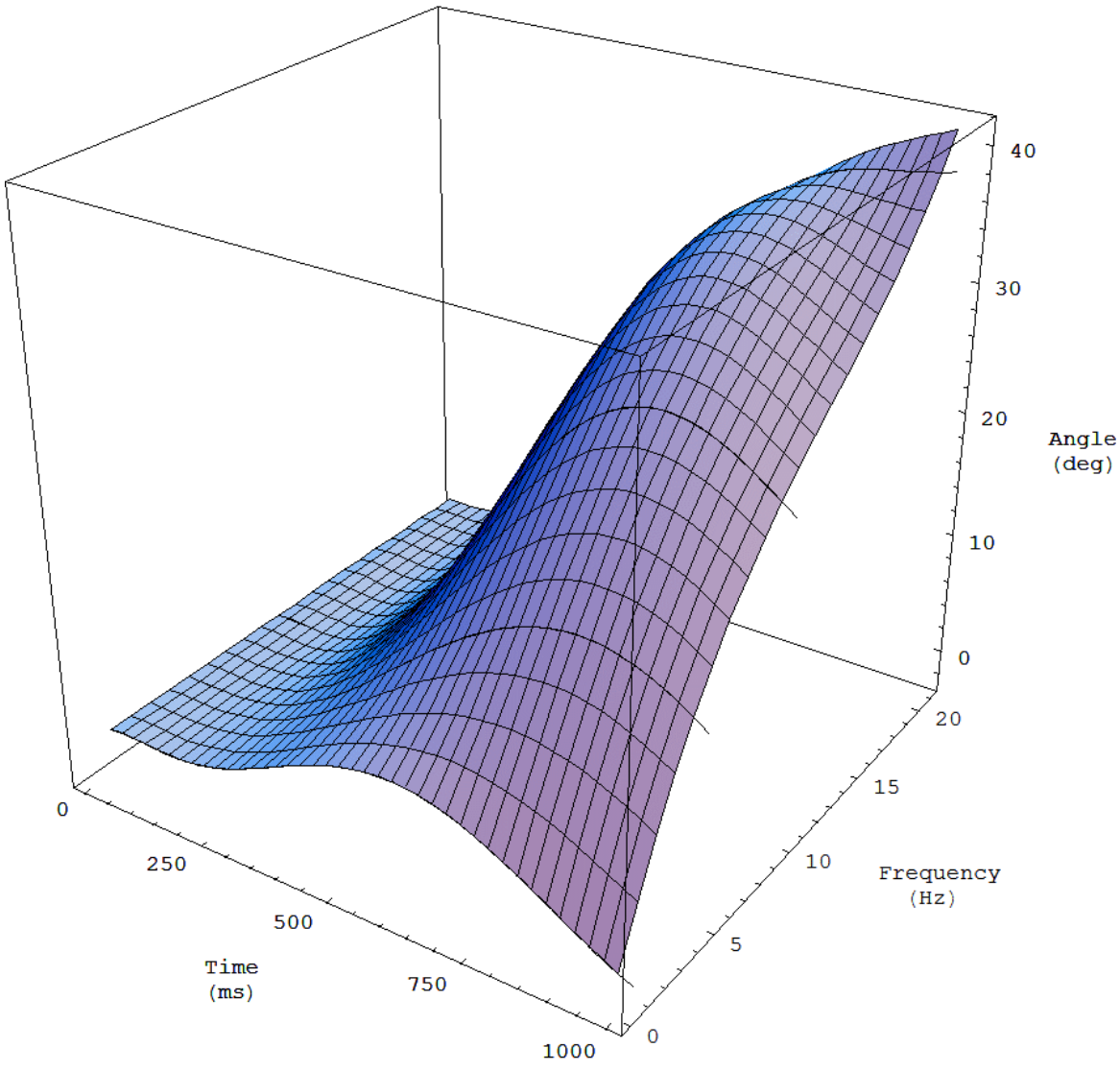

Figure 1–2: Leg angle generated with a constant frequency for one second with a 100 μs wide pulse delivered at 40 volts. The stimulation frequencies were 1, 5, 10, and 20 Hz.

To address the uncertainties of non-model-based NMES, two categories of nonlinear controllers were implemented; an extremum seeking numerical method, and a robust method.

Extremum seeking is an alternative non-model-based method that has been applied to a variety of engineering systems beginning at least five decades ago [19–23] that has experienced a resurgence over the past two decades [24]. The return to popularity of extremum seeking methods is based on the simplicity of approach (e.g., compared to implementing a neural network) and the non-model-based characteristic. Extremum seeking is an attractive approach for applications where the response of the system is dictated by a nonlinear behavior that is difficult to model and has a local minimum or maximum [24].

This thesis explores the use of an extremum seeking method to determine NMES parameters for setpoint regulation of a human knee/lower limb (the method could be applied to other muscle groups without loss of generality). Specifically, an error signal is defined between the actual angle of the knee and some known desired angle. The angular position of the knee/lower limb is related to some set of stimulation parameters through some unknown mapping (i.e., a muscle model). If multiple parameters were varied simultaneously, there would exist an infinite combination of stimulation parameters yielding the same angular position of the limb. Determining which parameters should be varied (e.g., some parameter variations have additional benefits such as reduced fatigue [25, 26]) is a topic of on-going research. The approach here is to set all the stimulation parameters to a constant except one so that a unique relationship exists between the single parameter and the knee/limb position. Specifically, efforts focus on using an extremum seeking algorithm to determine the optimal voltage (amplitude modulation) or optimal frequency (frequency modulation) to yield a desired knee/limb position. Other modulation schemes such as pulse width modulation

could also be explored using the exact same approach. An advantage of the developed approach is that only the upper and lower bounds on the voltage and frequency are required (i.e., a muscle model is not required). Experimental results are provided that indicated the desired knee/limb position is obtained within 0.7° of error for both frequency and voltage modulation. The experiments were developed as a self-test. That is, given a set of stimulation parameters the extremum seeking algorithm would determine an optimal voltage amplitude. The computed voltage amplitude was then used with the same stimulation parameters in a second experiment where the extremum seeking algorithm determined the corresponding frequency. The experiment showed that the computed frequency matched the preset frequency of the first experiment within one hertz

Recently, a new continuous feedback method (coined RISE for Robust Integral of the Sign of the Error in [27, 28]) has been developed that was proven to yield asymptotic tracking of nonlinear systems with unstructured uncertainty and bounded additive disturbances. The contribution here is to illustrate how the RISE controller can be applied for NMES systems. Implementing the RISE method required developing, and then rewriting, a muscle model in a form that adheres to previous RISE-based Lyapunov stability analyses. The performance of the nonlinear controller is experimentally verified for both the tracking and regulation of a human shank/foot complex by applying NMES across external electrodes attached to the distal-medial and proximal-lateral portion of the quadriceps femoris muscle group. The RISE controller used a voltage modulation scheme with a fixed frequency and a fixed pulse width. Other modulation strategies (e.g., frequency or pulse-width modulation) could have also been implemented (and applied to other skeletal muscle groups) without loss of generality. For these initial results, the regulation experiment indicates that the desired knee-joint angle can be regulated

within 0.5° of error, and the tracking experiment can be controlled within 3.5° of steady-state error.

In addition to developing two nonlinear control schemes, the electronic circuitry used for generating the electrical impulse delivered to the muscle was also developed. A requirement for the circuitry was that it needed to deliver a pulse train with a positive square pulse whose width was between $100 - 675$ μsecs. It must have a frequency range between $10 - 1000$ Hz and an amplitude between $1 - 150$ volts. An additional requirement was that the frequency and voltage must be able to respond to changes in the computed values at the control-sampling rate (1000 Hz). The circuitry described in the appendix also incorporates the interfacing of a load cell for isometric experiments. All experiments were non-isometric and use a pulse train with a 100 μsec positive square pulse and then modulate either the frequency or the voltage.

CHAPTER 2
EXTREMUM SEEKING CONTROL SCHEME

An optimal extremum seeking approach is developed in this chapter to identify frequency and voltage modulation parameters for a neuromuscular electrical stimulation control objective. The control objective is to externally apply optimally varied voltage or frequency modulation parameters to a human quadriceps muscle to generate a desired knee-joint angle. Experimental results are provided to illustrate the limb positioning performance of a real-time extremum seeking routine (i.e., Brent's Method).

The focus of this research was to determine the NMES parameters for a regulation experiment of a human knee-joint (the method could be applied to other muscle groups without loss of generality). Specifically, an error signal was defined between the actual angle of the knee and some known desired angle. The angular position of the knee-joint is related to some set of stimulation parameters through some unknown mapping (i.e., a muscle model). A combination of stimulation parameters yields the same angular position of the limb if multiple parameters are varied simultaneously. Which parameters should be varied (e.g., some parameter variations have additional benefits such as reduced fatigue [25, 26]) is a topic of on-going research. The approach presented focuses on setting all but one stimulation parameter constant so that a unique relationship exists between the single parameter and the knee-joint angle.

The extremum seeking method is based on an iterative numerical method. The controller regulates the test subject's quadriceps muscle via frequency or voltage modulation in order to move the knee-joint to 45°. Extremum seeking is

an alternative non-model-based method that has been applied to a variety of engineering systems beginning at least five decades ago [19–23] that has experienced resurgence over the past two decades [24]. The return to popularity of extremum seeking methods is based on the simplicity of the approach (e.g., compared to implementing a neural network) and its non-model-based characteristic. It is also an attractive approach for applications where the response of the system is dictated by a nonlinear behavior that is difficult to model and where the nonlinearity has a local minimum or a maximum [24]. The control method is used to determine the optimal voltage or frequency needed to generate the desired knee-joint angle. Other modulation schemes such as pulse width modulation could also be explored with the exact same approach.

Three extremum search algorithms were investigated as candidates for control of NMES; Brent's Method [29], a Downhill Simplex Method [29], and Krstic's Perturbation Method [30]. The decision for the control method was based on five criteria:

- It must not require a plant (a muscle model).
- It does not require tuning of control gains.
- It must quickly converge on a solution.
- It must be robust in the sense that its performance is independent of the patient's muscle dynamics.
- It must allow for at least one independent variable.

Using the above criteria, the Simplex method was not chosen as it is more appropriate for systems with multiple independent variables. The Perturbation Method was not chosen (even though it has proven stability results) because it is very slow to converge on a solution. Brent's iterative numerical method was chosen because it adhered to all of the above criteria.

2.1 Control Objective

The objective of the controller is to regulate the angle of a person's knee-joint through NMES of the quadriceps muscle undergoing non-isometric contractions. To quantify this objective, an angular knee position error, denoted by $e(t) \in \mathbb{R}$, is defined as

$$e(t) = q(t) - q_d(t) \tag{2–1}$$

where $q_d(t) \in \mathbb{R}$ denotes a constant known desired angular knee position. To position the knee (and hence limb) at the desired angle requires a unique contraction force be elicited by a combination of stimulation parameters. For an amplitude modulation strategy, the stimulation frequency is held constant and the voltage amplitude is varied. Therefore, a challenge in achieving the objective in (2–1) is that a desired voltage must be determined that ensures $v(t) \to v_d^*$ where $v_d^* \in \mathbb{R}$ is an unknown positive constant representing the unknown desired voltage corresponding to the desired knee-joint angle $q_d(t)$. The subsequent development is not based on an assumed muscle model, but a requirement for extremum seeking methods is that a unique voltage (or frequency) exists that will minimize the regulation error $e(t)$ (i.e., the contraction force of the muscle is not saturated). The following development is provided for amplitude modulation without loss of generality. Frequency and amplitude modulation methods are presented in the experimental results in Section 2.3.

2.2 Extremum Generation

Several extremum search algorithms (e.g. Brent's Method [29], a Downhill Simplex Method [29], and Krstic's Perturbation Method [30], etc.). can be utilized to show that if $v(t) \to v_d^*$, then the angular knee position error is minimized. For example, Brent's Method only requires measurement of the output function (i.e., $e(t)$ in (2–1)) and two initial guesses that enclose the unknown value for v_d^* (the two initial guesses are not required to be close to the value of v_d^*). Brent's Method

then uses an inverse parabolic interpolation algorithm and measurements of $e(t)$ to generate estimates for v_d^* until the estimates converge. Specifically, an objective function, denoted by $\varphi(q(t)) \in \mathbb{R}$, is defined as

$$\varphi(q) \triangleq \frac{1}{2}(q - q_d)^T (q - q_d). \tag{2–2}$$

The objective function in (2–2) has a unique minimum at $q(t) = q_d(t)$. The unknown mapping $\Pi_1(\cdot) : \mathbb{R} \to \mathbb{R}$ between the applied voltage and resulting limb position can be used to rewrite (2–2) as

$$\varphi(v) = \frac{1}{2}(\Pi_1(v) - \Pi_1(v_d^*))^T (\Pi_1(v) - \Pi_1(v_d^*)). \tag{2–3}$$

Under the assumption that $\Pi_1(\cdot)$ is monotonic, a unique minimum at $v(t) = v_d^*$ corresponds to a unique minimum at $q(t) = q_d(t)$. A variety of standard optimization routines (e.g., FMINUNC from the MATLAB optimization) could potentially be utilized to locate the minimum of $\varphi(q(t))$. However, because $q(t)$ cannot be directly manipulated and because the limb has associated dynamics, a delay function must be included in the optimization routine. Specifically, once the optimization routine generates a new voltage $v(t)$, the routine must pause until the dynamics reach steady-state at which point the resulting knee-joint angle is evaluated. In the following experimental results, the optimization routine included a delay that was experimentally determined to be sufficient for the limb dynamics to reach steady-state. More sophisticated methods such as a sliding window could also be explored.

The numerically-based extremum generation formula for computing the optimal voltage amplitude (for a given frequency, pulse width, and waveform) that minimizes the angular knee position error can be described as follows [31].

- Step 1. Three initial best-guess estimates, denoted by λ_1, λ_2, $\lambda_3 \in \mathbb{R}$, are selected where λ_1 is the best-guess estimate for a lower bound on the optimal

voltage, λ_3 is the best-guess estimate for an upper bound on the optimal voltage, and λ_2 is the best-guess estimate for the optimal voltage, where $\lambda_2 \in (\lambda_1, \lambda_3)$. The muscle is stimulated with $v(t) = \lambda_2$. In the experimental results presented in this paper, a positive square wave with a 100 μsec pulse width was applied for five seconds at a preset frequency (i.e., 20 Hz).

- Step 2. The algorithm waits for the limb dynamics to reach steady-state.
- Step 3. The next voltage amplitude is determined from the following expression

$$\lambda_4 = \lambda_2 - \frac{1}{2}\frac{g_1}{g_2} \tag{2–4}$$

where g_1, $g_2 \in \mathbb{R}$ are constants defined as

$$\begin{aligned} g_1 = (\lambda_2 - \lambda_1)^2[\varphi(\lambda_2) - \varphi(\lambda_3)] \\ - (\lambda_2 - \lambda_3)^2[\varphi(\lambda_2) - \varphi(\lambda_1)] \end{aligned} \tag{2–5}$$

$$\begin{aligned} g_2 = (\lambda_2 - \lambda_1)[\varphi(\lambda_2) - \varphi(\lambda_3)] \\ - (\lambda_2 - \lambda_3)[\varphi(\lambda_2) - \varphi(\lambda_1)] \end{aligned} \tag{2–6}$$

where $\lambda_i \ \forall i = 1, 2, 3$ are determined from the first two steps. Specifically, λ_i and $\varphi(\lambda_i)$ are substituted into (2–4)-(2–6) and the resulting expression yields the next best-guess for v_d^* denoted by $\lambda_4 \in \mathbb{R}$. The muscle is stimulated with $v(t) = \lambda_4$.

- Step 4. The algorithm waits for the limb dynamics to reach steady-state.
- Step 5. The resulting steady-state limb position corresponding to $v(t) = \lambda_4$ (denoted by $e(\lambda_4)$) is compared to the resulting limb position corresponding to $v(t) = \lambda_2$ (denoted by $e(\lambda_2)$). Based on the conditions shown in Table 2–1 the stimulation bounds are modified. If $e(\lambda_4) \geq e(\lambda_2)$ and $\lambda_2 > \lambda_4$ or if $e(\lambda_2) \geq e(\lambda_4)$ and $\lambda_4 > \lambda_2$, then the three new estimates used to construct a new parabola are λ_2, λ_3, λ_4. If $e(\lambda_4) \geq e(\lambda_2)$ and $\lambda_4 > \lambda_2$ or if $e(\lambda_2) \geq e(\lambda_4)$

Table 2–1: Determining whether to change the upper or lower bound.

Condition 1: Lower Bound too Low		
Current Error $\geq$ Previous Error	AND	Previous Voltage > Current Voltage
OR		
Previous Error $\geq$ Current Error	AND	Current Voltage > Previous Voltage

Condition 2: Upper Bound too High		
Current Error $\geq$ Previous Error	AND	Current Voltage > Previous Voltage
OR		
Previous Error $\geq$ Current Error	AND	Previous Voltage > Current Voltage

and $\lambda_2 > \lambda_4$, then the three new estimates used to construct a new parabola are λ_1, λ_2, λ_4.

- Step 6. Repeat Steps 3-5 for successive $\lambda_i \; \forall i = 5, 6, ...$, where the three estimates determined from Step 5 are used to construct a new parabola. Steps 3-5 are repeated until the difference between the new upper and lower estimates is below some predefined, arbitrarily small threshold.

2.3 Experimental Results

Two NMES experiments were performed using Brent's Method as the controller. The first experiment involved positioning the knee-joint to a desired angle via. voltage modulation (VM). The second experiment involved frequency modulation (FM) whose purpose was a self-test of the control method.

2.3.1 Experimental Testbed

All the experiments were conducted on a modified commercial leg curl and extension machine (LEM) and a custom computer controlled stimulation circuit. The picture of the testbed is shown in Fig. 2–1. The LEM was modified to include two 5000 pulse-per-revolution optical encoders with incremental quadrature output of $\pm$A and $\pm$B channels (one encoder per leg). The precision of the encoders

Figure 2–1: Leg curl and extension machine after modifications.

allows for a resolution of 0.018° with a frequency response of 150 kHz. The LEM allows seating adjustments to ensure the rotation of the knee is about the encoder axis. For the experiment a 4.5 kg (10 lb.) load was attached to the weight bar of the LEM, and a mechanical stop was used to prevent hyperextension.

A custom stimulation circuit was interfaced with a ServoToGo data acquisition card. The data acquisition was performed at 1000 Hz and consisted of a single encoder whose output was used to determine the knee angle, and two digital-to-analog signals were used as input to the custom stimulation circuitry that produces a 100 μsec positive square pulse between $3 - 1000$ Hz with a voltage output between $1 - 100$ volts peak. The I/O card is contained in a Pentium IV PC hosting the real-time operating system QNX. The RISE algorithm was implemented in C++, and the resulting real-time executable was accessed through the QMotor 3.0 Graphical User Interface [32].

In the experiment, bipolar self-adhesive neuromuscular stimulation electrodes were placed over the distal-medial and proximal-lateral portion of the quadriceps femoris muscle group and connected to the custom stimulation circuitry. Prior to participating in the study, written informed consent was obtained from all subjects, as approved by the Institutional Review Board at the University of Florida. All test subjects were healthy males between the ages of 24 and 50. Each test subject was instructed to relax as much as possible and to allow the stimulation to control the limb motion (i.e., the subjects were not supposed to influence the leg motion voluntarily).

2.3.2 Experimental Setup

An experiment was performed using Brent's Method (Section 2.2) to determine the optimal voltage amplitude, given a positive square wave with a pulse width of 100 μsec and frequency of 20 Hz. Once the seeking routine determined the optimal voltage amplitude, a frequency modulation experiment was performed using the computed voltage from the first experiment along with the same 100 μsec pulse width. The extremum seeking method was used in the second experiment to determine the optimal corresponding frequency. Since the voltage magnitude from the first experiment is used in the second experiment, the optimal frequency in the second experiment should be approximately 20 Hz. The following results indicate that in both tests the extremum seeking algorithm was able to minimize the angular knee position regulation error, and that the frequency seeking strategy converged near the frequency used in the first experiment.

2.3.3 Optimal Voltage Seeking Results

Following Step 1 in the procedure outlined in Section 2.2, the three initial best-guess estimate voltages, λ_1, λ_2, λ_3 were selected as

$$\lambda_1 = 20.0 \qquad \lambda_2 = 30.0 \qquad \lambda_3 = 55.0.$$

The muscle was stimulated with a 30 volt positive square wave pulse train with a fixed 100 μsec pulse width at 20 Hz. The pulse train was applied for 5 seconds to ensure the limb dynamics reach steady-state. The 5-second delay is a simple method to ensure the dynamics reach steady-state based on previous experience with the experimental testbed and test subject; however, several alternative methods could have also been used such as a sliding window method that monitors peak to peak oscillations. During the five seconds of stimulation, the knee-joint angle measurements were recorded at 1000 Hz. The angle recorded at the end of the five seconds (i.e., the steady-state value) was recorded and used as an input (i.e., Step 3 in Section 2.2) to Brent's Method to compute the next stimulation value, λ_4. The knee angle measurement was recorded after five seconds of stimulation with $v(t) = \lambda_4$ and used to compute the next stimulation value based on Step 5 in Section 2.2. According to Step 6, Steps 3-5 were repeated until the algorithm converged within a tolerance of the desired angle. Representative results (Fig. 2–2) show five iterations of Steps 3-5 were implemented until the algorithm converged to 44.7 volts. Fig. 2–2 indicates the desired knee angle (short dashed) of 45°, the actual leg angle (solid), and the output voltage (long dashed) computed from Brent's Method.

As shown in Fig. 2–2 the first best-guess for λ_2 was 30 volts which yielded a steady-state knee angle of approximately 6.3°. The next stimulation voltage, determined from the joint angle error as $\lambda_4 = 37.6$ volts, generated a knee-joint angle of 29.7°. After three additional iterations the knee-joint angle was approximately 44.1° which was within the desired tolerance. Table 2–2 summarizes the computed voltage levels and the resulting knee angle. Using four test subjects, a total of seven VM experiments were performed. Fig. 2–3 shows a second example of Brent's Method overshooting the desired angle before converging to the solution. The RMS errors, standard deviation, and steady-state errors for the seven VM

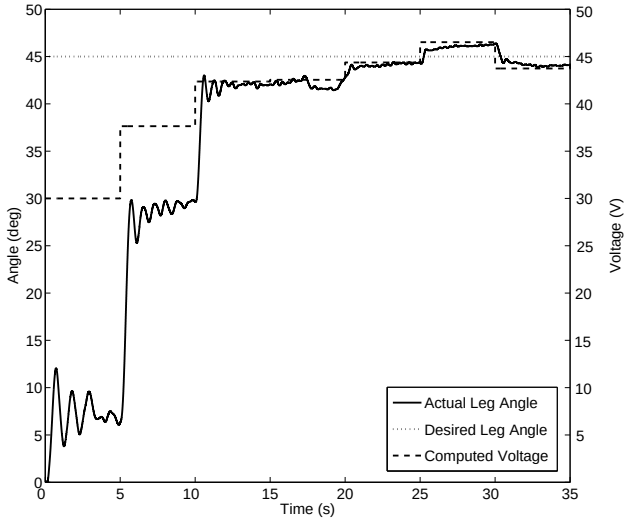

Figure 2–2: Online computed voltage (long dashed), desired leg angle (short dashed), and actual leg angle (solid).

Table 2–2: Knee-joint angle controlled by voltage

Time [s]	Angle [deg]	Voltage [V]
0.00	0.0	30.0
5.00	6.3	37.6
10.00	29.7	42.4
15.00	42.1	42.5
20.00	42.8	44.4
25.00	44.3	46.5
30.00	46.4	43.7
35.00	44.1	44.7

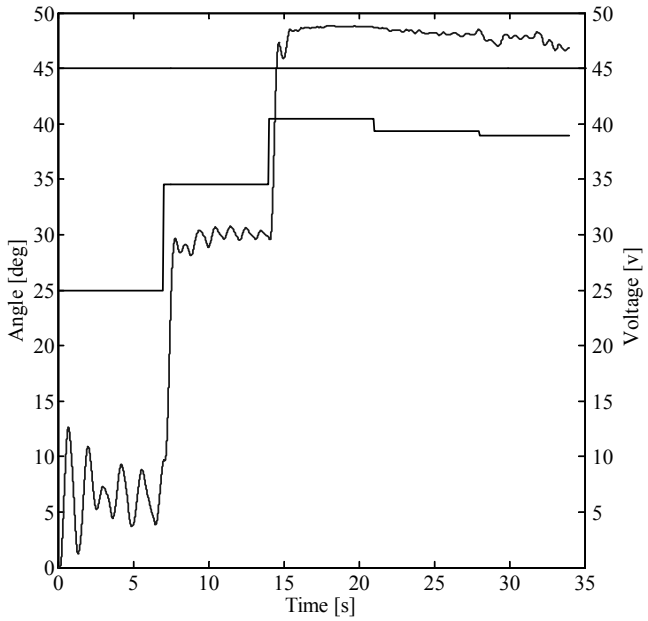

Figure 2–3: Brent's Method overshooting the desired angle before converging towards the solution using VM.

experiments are shown in Table 2–3. The point in time when the system achieved steady-state was estimated to occur at 3/4 of the total experiment time, hence the steady-state errors use data from the final 1/4 of the stimulation period.

2.3.4 Optimal Frequency Seeking Results

A second experiment was performed where the extremum seeking algorithm was used to determine the desired frequency using FM for a given voltage amplitude, waveform, and pulse width. Motivation for the FM experiment was a self-test to demonstrate the ability of using the extremum seeking method for frequency modulation and to compare the results between the two experiments. Specifically, using a frequency of 20 Hz in the previous VM experiment, the extremum seeking algorithm converged to 44.7 volts. Therefore, in order to determine the validity of Brent's Method as a controller, the voltage for the FM experiment was set to 44.7 volts. Using the previous voltage, the extremum seeking algorithm in the FM

Table 2–3: RMS error and steady-state error for Brent's Method using VM

Test Subject	Leg	RMS Error	Steady-state Error (RMS)	Max. Steady-state Error (deg.)	
1	Left	20.766	0.771	1.062	
1	Right	19.396	3.188	3.528	
2	Left	19.107	5.664	6.876	
2	Right	19.856	5.278	6.372	
3	Left	16.130	1.490	1.404	
3	Right	14.255	2.894	3.600	
4	Left	12.293	3.762	1.062	
		17.400	3.293	3.414	Mean
		2.972	1.672	2.264	Standard Deviation

experiment should converge to 20 Hz. The FM experiment was performed after the test subject was given a 2 minute rest period.

Following Step 1 of the procedure outlined in Section 2.2, the three initial best-guess estimate frequencies, λ_1, λ_2, λ_3 were selected as

$$\lambda_1 = 15 \qquad \lambda_2 = 18 \qquad \lambda_3 = 25.$$

The muscle was stimulated with a 44.7 volt (i.e., the optimal voltage corresponding to a 20 Hz pulse train from the VM experiment) positive square wave pulse train with a fixed 100 μsec pulse width at a frequency of $f(t) = 18$ Hz for 5 sec. The angle recorded at the end of the five seconds (i.e., the steady-state value) was recorded and used as an input (i.e., Step 3 in Section 2.2) to Brent's Method to compute the next stimulation value, λ_4. The knee angle measurement was recorded after five seconds of stimulation with the stimulation frequency $f(t) = \lambda_4$ and used to compute the next stimulation value based on Step 5 in Section 2.2. According to Step 6, Steps 3-5 were repeated until the algorithm converged within a tolerance of the desired angle. As indicated in Figure 2–4, five iterations of Steps 3-5 were implemented until the algorithm converged to within a tolerance. Figure 2–4

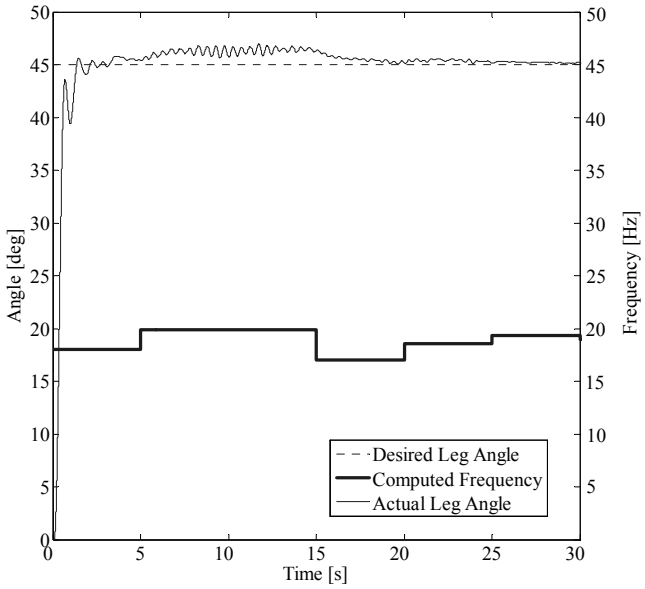

Figure 2–4: Online computed frequency (bold solid), desired leg angle (short dashed), and actual leg angle (solid).

indicates the desired knee angle (short dashed) of 45°, the actual knee angle (solid), and the output frequency (bold solid) computed from Brent's Method.

Fig. 2–4 indicates that the initial frequency of 18 Hz generated a steady state joint angle of 45.4°. After five iterations, the algorithm converged to 19.0 Hz and 45.2°. Table 2–4 summarizes the results from the frequency experiment and illustrates that small changes in the frequency produce measurable changes in the joint angle. The same four test subjects used in the VM experiments were used for seven FM experiments. Fig. 2–5 shows a second example of Brent's Method overshooting the desired angle before converging to the solution. The RMS errors, standard deviation, and steady-state errors for the seven FM experiments are shown in Table 2–5. The point in time when the system achieved steady-state was estimated to occur at 3/4 of the total experiment time, hence the steady-state errors use data from the final 1/4 of the stimulation period.

Table 2–4: Knee-joint angle controlled by frequency

Time [s]	Angle [deg]	Frequency [Hz]
0.00	0.0	18.0
5.00	45.4	19.9
10.00	45.7	19.9
15.00	46.3	17.1
20.00	45.2	18.6
25.00	45.2	19.4
30.00	45.2	19.0

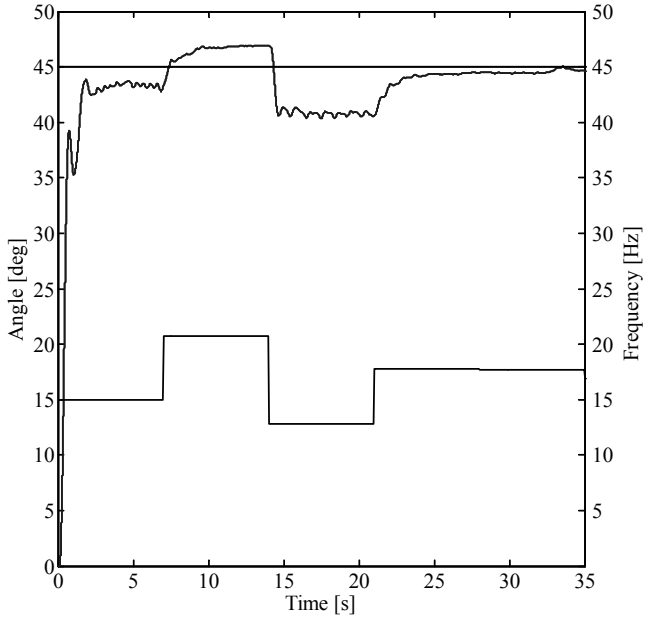

Figure 2–5: Brent's Method converging on the solution using FM.

Table 2–5: RMS error and steady-state error for Brent's Method using FM

Test Subject	Leg	RMS Error	Steady-state Error (RMS)	Max. Steady-state Error (deg.)	
1	Left	4.906	0.855	1.494	
1	Right	5.091	1.885	0.594	
2	Left	4.984	1.819	1.368	
2	Right	5.135	0.940	3.078	
3	Left	5.740	1.914	2.088	
3	Right	4.894	1.786	2.268	
4	Left	4.661	0.377	0.522	
		5.058	1.638	1.630	Mean
		0.313	0.582	0.854	Standard Deviation

2.4 Discussion

The results from both experiments were promising. Specifically, the experimental results indicated that with no muscle model (only upper and lower frequency and voltage amplitudes were required), the extremum seeking algorithm could determine the appropriate stimulation within approximately five iterations. The extremum seeking algorithm was applied for both voltage modulation and frequency modulation to obtain a less than 0.9° degree steady-state limb/knee positioning error. The experiments were constructed to perform a self-test. By using the voltage amplitude determined from the first experiment, the frequency algorithm in the second experiment converged to within one hertz of the frequency used in the first experiment. Different extremum seeking algorithms could be applied for different results. Hence, the idea of using an optimal extremum seeking algorithm to determine stimulation parameters for NMES applications seems promising.

2.5 Concluding Remarks

An extremum seeking NMES approach was implemented to stimulate the human quadriceps muscle group. A modified version of Brent's Method was implemented as the extremum seeking routine to determine voltage or frequency

modulation parameters that would yield a desired angular knee position. This method only required measurements of the resulting knee angle, and some knowledge of upper and lower bounds on the voltage or frequency settings. Experimental results were obtained that indicated the desired knee/limb position could be obtained within a 0.9° tolerance. In one experiment the algorithm was applied to determine the voltage amplitude where the remaining stimulation parameters were fixed, and a second experiment was performed where the algorithm determined the desired frequency.

CHAPTER 3
NONLINEAR CONTROL SCHEME

A nonlinear control method is developed in this chapter that uses neuromuscular electrical stimulation to control the human quadriceps femoris muscle undergoing non-isometric contractions. The objective of the controller is to position the lower limb of a human along a time-varying trajectory or to a desired setpoint. The developed controller does not require a muscle model and can be proven to yield asymptotic stability for a nonlinear muscle model in the presence of bounded nonlinear disturbances. Performance of the controller is illustrated in the provided experimental results.

3.1 Robust Integral Sign of the Error

The research presented here illustrates the performance of a computer controlled NMES method for both tracking and regulation of a human knee-joint angle. The method could be applied to other muscle groups without loss of generality. The NMES controller is based on the recently developed Robust Integral Sign of the Error (RISE) technique that uses an error signal defined between the actual angle of the knee and some known desired angle. One of the motivating factors for implementing the RISE controller is that the method does not depend on muscle-model knowledge, and Lyapunov-based stability analysis methods have been developed that prove asymptotic stability for dynamic systems subject to general bounded disturbances [27, 28]. Significant research efforts have focused on the use of neural network-based controllers [10–18]. Nonlinear neural network methods provided a framework that allowed the performance, robustness, and stability of the developed NMES controllers to be investigated without linearization assumptions. However, all of the previous neural network-based NMES controllers are limited

to a uniformly ultimately bounded result because of the inevitable residual nonlinear function approximation error. Additionally, neural networks may exhibit performance degradation during the transient phase while the estimates update. In comparison to other non-model-based approaches such as PD/PID controllers [2–6], the RISE method is a robust controller that was proven to yield asymptotic tracking of nonlinear systems with unstructured uncertainty and bounded additive disturbances. In comparison to optimal methods such as extremum seeking, the RISE controller does not require the global maximum assumption for the torque/voltage curve, and does not require iterative steps that are delayed by the transient response of the muscle and limb dynamics. In order to implement the RISE controller a muscle model is developed and then rewritten in a form that adheres to previous RISE-based Lyapunov stability analyses. The performance of the nonlinear controller is experimentally verified for both the tracking and regulation of a human leg/shank by applying the controller as a voltage potential across external electrodes attached to the distal-medial and proximal-lateral portion of the quadriceps femoris muscle group. The RISE controller is implemented by a voltage modulation scheme with a fixed frequency and a fixed pulse width. Other modulation strategies (e.g., frequency or pulse-width modulation) could have also been implemented (and applied to other skeletal muscle groups) without loss of generality.

The experimental results for the regulation scenario are described in Section 3.4.2, and the tracking experimental results are provided in Section 3.4.3. These preliminary experimental results indicate that the desired knee-joint angle can be regulated within 0.5° of error for the fixed angle experiment, and within 3.5° of steady-state error for the tracking experiment.

3.2 Muscle Activation and Limb Model

The total knee-joint dynamics can be modeled as [5]

$$M_I + M_e + M_g + M_v + \tau_d = \tau. \tag{3–1}$$

In 3–1, $M_I(\ddot{q}) \in \mathbb{R}$ denotes the inertial effects of the shank-foot complex about the knee-joint, $M_e(q) \in \mathbb{R}$ denotes the elastic effects due to joint stiffness, $M_g(q) \in \mathbb{R}$ denotes the gravitational component, $M_v(\dot{q}) \in \mathbb{R}$ denotes the viscous effects due to damping in the musculotendon complex [33], $\tau_d(t) \in \mathbb{R}$ represents unknown unmodelled bounded disturbances (e.g., fatigue, signal and response delays, unmodelled phenomena), and $\tau(t) \in \mathbb{R}$ denotes the torque produced at the knee-joint.

The inertial and gravitational effects in (3–1) can be modelled as

$$M_I(\ddot{q}(t)) = J\ddot{q}(t), \qquad M_g(q(t)) = -mgl\sin(q(t)),$$

where $q(t)$, $\dot{q}(t)$, $\ddot{q}(t) \in \mathbb{R}$ denote the angular (Fig. 3–1) position, velocity, and acceleration of the lower shank about the knee-joint, respectively, $J \in \mathbb{R}$ denotes the unknown inertia of the combined shank and foot, $m \in \mathbb{R}$ denotes the unknown combined mass of the shank and foot, $l \in \mathbb{R}$ is the unknown distance between the knee-joint and the lumped center of mass of the shank and foot, and $g \in \mathbb{R}$ denotes the gravitational acceleration.

The elastic effects are modelled on the empirical findings by Ferrarin and Pedotti in [33] as

$$M_e(q) = -k_1(\exp(-k_2 q(t)))(q(t) - k_3), \tag{3–2}$$

where k_1, k_2, $k_3 \in \mathbb{R}$ are unknown positive coefficients. As shown in [5], the viscous moment $M_v(\dot{q})$ can be modelled as

$$M_v(\dot{q}(t)) = B_1 \tanh(-B_2\dot{q}(t)) - B_3\dot{q}(t), \tag{3–3}$$

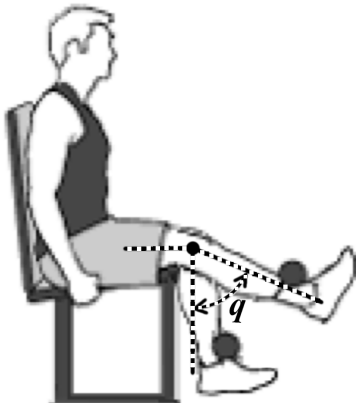

Figure 3–1: Knee-joint angle defined by q.

where B_1, B_2, and $B_3 \in \mathbb{R}$ are unknown positive constants.

The torque produced about the knee is controlled through muscle forces that are elicited by NMES. For simplicity (and without loss of generality), the development in this paper focuses on producing knee torque through forces, denoted by $F(t) \in \mathbb{R}$, generated by electrical stimulation of the quadriceps (i.e., we do not consider antagonistic muscle forces). The knee torque is related to the quadriceps force as

$$\tau(t) = \zeta(q(t))F(t), \tag{3–4}$$

where $\zeta(q(t)) \in \mathbb{R}$ denotes a positive moment arm that changes with the extension and flexion of the leg as shown in studies by [34] and [35]. As indicated in [34], the moment arm $\zeta(q(t))$ has unique values for a given range of motion, while in [35], the moment arm's unique values are obtained for the entire range of motion.

The muscle force $F(t)$ is generated by the available actin and myosin filament binding sites in the muscle fibers. The voltage applied to the muscle alters the calcium ion concentration which influences the actin-myosin binding. The relationship between the muscle force and the applied voltage is denoted by the unknown function $\eta(t) \in \mathbb{R}$ as

$$F(t) = \eta(t)V(t), \tag{3–5}$$

where $V(t) \in \mathbb{R}$ is the voltage applied to the quadriceps muscle by electrical stimulation. While exact force versus voltage models are debatable and contain parametric uncertainty, the generally accepted empirical relationship between the applied voltage (or similarly, current, frequency, or pulse width) is well established.

The following properties have been exploited in subsequent control development.

Property 1: The unknown disturbance $\tau_d(t)$ is bounded and its first and second derivatives with respect to time exist and are bounded.

Property 2: The moment arm $\zeta(q(t))$ is a continuously differentiable, positive, monotonic, bounded function [35], and empirical data indicates the function $\eta(t)$ is also a continuously differentiable, positive, monotonic, and bounded function.

3.3 Control Development

The objective in this paper is to develop a NMES controller to produce a knee torque trajectory that will enable a human shank to track a desired trajectory, denoted by $q_d(t) \in \mathbb{R}$. Without loss of generality, the developed controller is applicable to different stimulation protocols (i.e., voltage, frequency, or pulse width modulation). To quantify the objective, a position tracking error, denoted by $e_1(t) \in \mathbb{R}$, is

$$e_1(t) = q_d(t) - q(t), \tag{3–6}$$

where $q_d(t)$ is an a priori trajectory which is designed such that $q_d(t)$, $q_d^i(t) \in \mathcal{L}_\infty$, where $q_d^i(t)$ denotes the i^{th} derivative for $i = 1, 2, 3, 4$. To facilitate the subsequent analysis, filtered tracking errors, denoted by $e_2(t)$ and $r(t) \in \mathbb{R}$, are defined as

$$e_2(t) = \dot{e}_1(t) + \alpha_1 e_1(t), \tag{3–7}$$

$$r(t) = \dot{e}_2(t) + \alpha_2 e_2(t), \tag{3–8}$$

where α_1, $\alpha_2 \in \mathbb{R}$ denote positive constants. The filtered tracking error $r(t)$ is introduced to facilitate the closed-loop error system development and stability analysis but is not used in the controller because of a dependence on acceleration measurements.

After multiplying (3–8) by J and utilizing the expressions in (3–1) and (3–4) – (3–7), the following expression can be obtained:

$$Jr = W - \Omega V + \tau_d, \tag{3–9}$$

where $W(\dot{e}_1, e_2, t) \in \mathbb{R}$ is an auxiliary signal defined as

$$W = J(\ddot{q}_d + \alpha_1 \dot{e}_1 + \alpha_2 e_2) + M_e + M_g + M_v, \tag{3–10}$$

and the continuous, positive, monotonic, and bounded (see Property 2) auxiliary function $\Omega(q, t) \in \mathbb{R}$ is defined as

$$\Omega = \zeta \eta. \tag{3–11}$$

After multiplying (3–9) by $\Omega^{-1}(q, t) \in \mathbb{R}$, the following expression is obtained:

$$J_\Omega r = W_\Omega - V + \tau_{d\Omega}, \tag{3–12}$$

where $J_\Omega(q, t) \in \mathbb{R}$, $W_\Omega(\dot{e}_1, e_2, t) \in \mathbb{R}$, and $\tau_{d\Omega}(q, t) \in \mathbb{R}$ are defined as

$$J_\Omega = \Omega^{-1} J, \qquad W_\Omega = \Omega^{-1} W, \qquad \tau_{d\Omega} = \Omega^{-1} \tau_d.$$

To facilitate the subsequent stability analysis, the open-loop error system for (3–12) can be determined as

$$J_\Omega \dot{r} = -\frac{1}{2} \dot{J}_\Omega r + N - \dot{V} - e_2, \tag{3–13}$$

where $N(e_1, e_2, r, t) \in \mathbb{R}$ denotes the unmeasurable auxiliary term

$$N = \dot{W}_\Omega + e_2 - \frac{1}{2} \dot{J}_\Omega r \ + \ \dot{\tau}_{d\Omega}(q, t). \tag{3–14}$$

To further facilitate the analysis, another unmeasurable auxiliary term, $N_d(q_d, \dot{q}_d, \ddot{q}_d, \dddot{q}_d, t) \in \mathbb{R}$, is defined as

$$N_d = \dot{J}_\Omega(q_d)\ddot{q}_d + J_\Omega(q_d)\dddot{q}_d + \dot{M}_e(q_d) + \dot{M}_g(q_d) + \dot{M}_v(q_d) + \dot{\tau}_{d\Omega}(q_d, t) \tag{3–15}$$

After adding and subtracting (3–15) to (3–13), the open-loop error system can be expressed as

$$J_\Omega \dot{r} = -\dot{V} - e_2 + \tilde{N} + N_d, \tag{3–16}$$

where the unmeasurable auxiliary term $\tilde{N}(e_1, e_2, r, t) \in \mathbb{R}$ is defined as

$$\tilde{N}(t) = N - N_d, \tag{3–17}$$

Using [36], the Mean Value Theorem is applied to develop the following upper bound

$$\left\| \tilde{N} \right\| \leq \rho\left(\|z\|\right)\|z\|, \tag{3–18}$$

where $z(t) \in \mathbb{R}^3$ is defined as

$$z(t) \triangleq [e_1^T \ e_2^T \ r^T]^T. \tag{3–19}$$

Based on (3–15), and the fact that $q_d(t)$, $q_d^i(t) \in \mathcal{L}_\infty \ \forall \ i = 1, 2, 3, 4$, the following inequalities can be developed

$$\|N_d\| \leq \zeta_{N_d} \qquad \left\| \dot{N}_d \right\| \leq \zeta_{\dot{N}_d}, \tag{3–20}$$

where ζ_{N_d} and $\zeta_{\dot{N}_d} \in \mathbb{R}$ are known positive constants.

The developed open-loop error system in (3–16) is now similar to the open-loop error system in [27, 28, 37, 38]. Based on the dynamics given in equations (3–1) – (3–5) the following RISE feedback controller $V(t)$ is employed as a means

to achieve the tracking objective:

$$V(t) \triangleq (k_s+1)e_2(t) - (k_s+1)e_2(t_0) + \int_{t_0}^{t} [(k_s+1)\alpha_2 e_2(\tau) + \beta sgn(e_2(\tau))]d\tau, \tag{3–21}$$

where k_s, $\beta \in \mathbb{R}$ denote positive constant adjustable control gains, and $sgn(\cdot)$ denotes the signum function.

Theorem: The controller given in (3–21) ensures that all system signals are bounded under closed-loop operation and that the position tracking error is regulated in the sense that

$$\|e_1(t)\| \to 0 \qquad \text{as} \quad t \to \infty, \tag{3–22}$$

provided the control gain k_s, introduced in (3–21) is selected sufficiently large, and β is selected according to the following sufficient condition:

$$\beta > \left(\zeta_{N_d} + \frac{1}{\alpha_2}\zeta_{\dot{N}_d}\right), \tag{3–23}$$

where ζ_{N_d} and $\zeta_{\dot{N}_d}$ are known positive constants.

The stability analysis and complete development of the RISE method can be found in [27, 28, 37, 38].

3.4 Experimental Results

Two experiments were performed using the RISE controller given in (3–21). The voltage controller was implemented through an amplitude modulation scheme composed of a variable amplitude positive square wave with a fixed pulse width of 100 μsec and fixed frequency of 100 Hz. The following results indicate that the RISE algorithm was able to minimize the knee angle error while dynamically tracking a desired trajectory.

3.4.1 Experimental Setup

The RISE experiment was performed using the testbed described in Appendix 2.3.1. For both experiments a 4.5 kg (10 lb.) load was attached to the weight bar of the exercise machine.

In each experiment, bipolar self-adhesive neuromuscular stimulation electrodes that were placed over the distal-medial and proximal-lateral portion of the quadriceps femoris muscle group of each subject and connected to the custom stimulation circuitry. Prior to participating in the study, written informed consent was obtained from all subjects, as approved by the Institutional Review Board at the University of Florida. Test subject 1 was a healthy 25 year old male, test subject 2 was a healthy 24 year old male, and test subject 3 was a healthy 50 year old male. Each test subject was instructed to relax as much as possible and to allow the stimulation to control the limb motion (i.e., the subjects were not supposed to influence the leg motion voluntarily).

To determine bounds on the test subject's response to stimulation, a calibration protocol was performed to determine appropriate upper and lower stimulation bounds. Specifically, an initial stimulation voltage was chosen that would generate a knee-joint angle of 25°. The pulse width was set at 100 μsec and delivered at 100 Hz. Stimulation voltage was linearly increased at the rate of 2 volts per second until the knee-joint angle reached 45°, at which point the voltage would linearly decrease. This ad-hoc strategy provides some indication of the muscle response to stimulation for the different subjects so that the voltage levels could be maintained within safe regions of operation. Fig. 3–2 shows the typical muscle excursion of the test subjects used for the regulation and tracking experiments.

3.4.2 Regulation Results

The initial stimulation voltage for subject 1 was based on the linear voltage test described previously (Fig. 3–2) which indicated that for subject 1, 25 volts

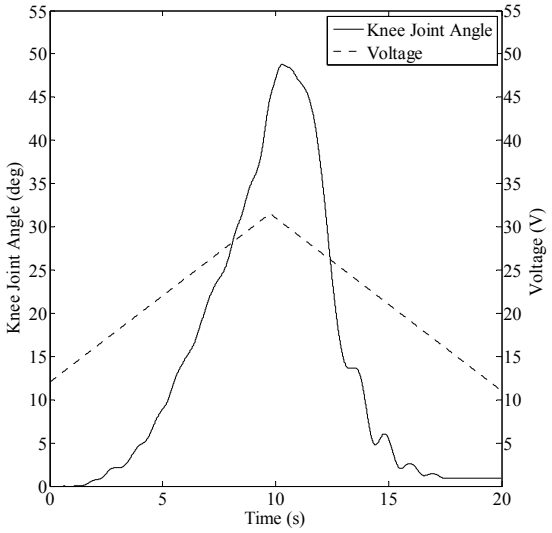

Figure 3–2: Typical muscle excursion of the test subjects used for the regulation and tracking experiments.

generated a knee-joint angle of 25°. The voltage was delivered as a positive square wave train with a fixed 100 μsec pulse width at 100 Hz.

For the regulation test, the desired knee angle shown in Fig. 3–3 increases from 0° to 45° in 2 seconds, in contrast to simply assigning a set-point of 45°, for comfort and safety of the study participants. The results obtained by the RISE method are shown in Fig. 3–3 which indicates the desired knee-joint angle (long dashed line) and the actual knee-joint angle (solid line). The computed output voltage is shown in Fig. 3–4 and a detail of the error (Fig. 3–5) shows that after 3 seconds the knee-joint angle was within 4°, and after 3.8 seconds the error never exceeded 0.5°. After 8 seconds the knee-joint angle was approximately 44.7°. Using three test subjects, a total of eight regulation experiments were performed (the first subject was tested on two separate days). The RMS errors, standard deviation, and steady-state errors for the eight experiments are shown in Table 3–1. The point in time when the system achieved steady-state was estimated to occur at 2/3 of the

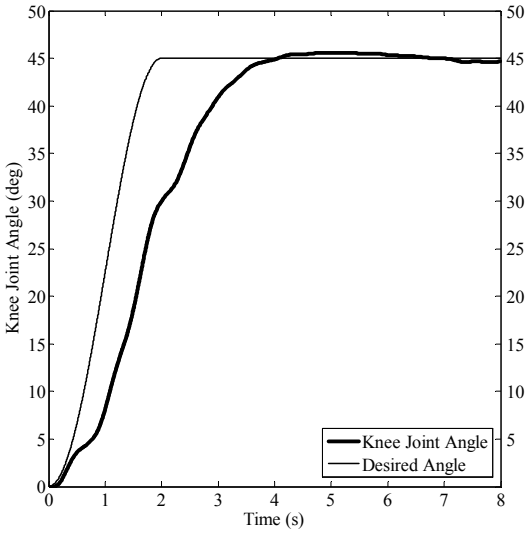

Figure 3–3: Regulation of knee joint angle using the RISE controller.

total experiment time, hence the steady-state errors use data from the final 1/3 of the stimulation period.

3.4.3 Tracking Results

The initial stimulation voltage for subject 2 was based on the linear voltage test described previously (Fig. 3–2) which indicated for subject 2, 18 volts generated a knee-joint angle of 25°. The voltage was delivered as a positive square wave train with a fixed 100 μsec pulse width at 100 Hz. The sinusoidal tracking profile in Fig. 3–6 was programmed for a minimum angle of 20° and a maximum of 45°. To ensure a smooth (and comfortable) stimulation behavior, two sinusoidal equations were used:

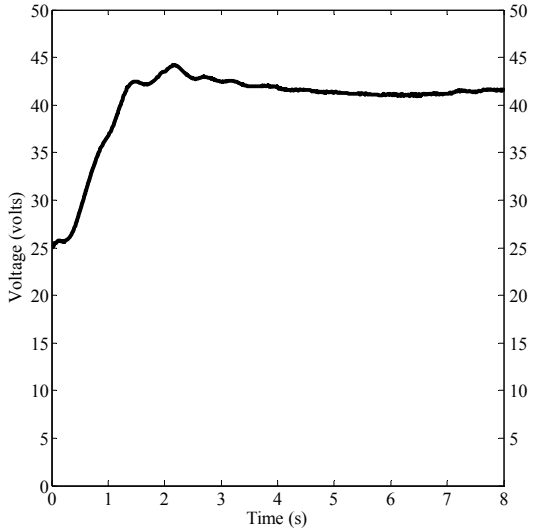

Figure 3–4: Regulation voltage using the RISE controller.

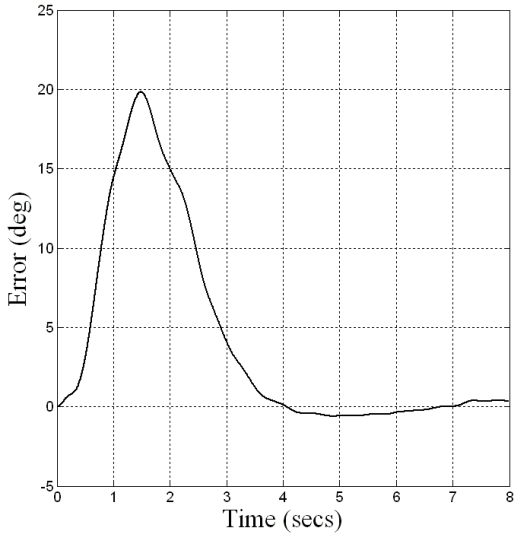

Figure 3–5: Regulation error of knee joint angle (desired angle minus actual angle).

Table 3–1: RMS and steady-state error for RISE regulation experiments

Test Subject	Leg	RMS Error	Steady-state Error (RMS)	Max. Steady-state Error (deg.)	
1	Left	17.079	0.473	0.232	
1	Right	17.913	0.336	0.643	
2	Left	17.980	0.432	0.502	
2	Right	17.997	0.198	0.355	
3	Left	18.692	0.462	0.340	
3	Right	18.734	0.349	0.320	
1	Left	18.610	0.332	0.312	
1	Right	18.593	0.728	0.385	
		18.200	0.414	0.386	Mean
		0.534	0.145	0.121	Standard Deviation

$$q_{d_1}(t) = \frac{\theta_d}{2} + \frac{\theta_d}{2}\left(\sin(\omega t + \frac{3}{2}\pi)\right), \tag{3–24}$$

$$q_{d_2}(t) = \left(\frac{\theta_d}{2} - \frac{\theta_m}{2}\right) + \left(\frac{\theta_d}{2} - \frac{\theta_m}{2}\right)\left(\sin(\omega t + \frac{3}{2}\pi)\right) + \theta_m, \tag{3–25}$$

where θ_m denotes the minimum knee-joint angle, θ_d represents the maximum knee-joint angle, and ω denotes $2\pi/T$, (T equaled the knee-joint period). The desired trajectory in (3–24) was used until $q_{d_1}(t) = \theta_d$, and then the desired trajectory was changed to $q_{d_2}(t)$ in (3–25).

A representative graph of the tracking experiment (Fig. 3–7). shows the desired knee angle (long dashed line) and the actual knee-joint angle (solid line). The computed output voltage is shown in Fig. 3–8 and a detail of the error (Fig. 3–9) shows a maximum transient error of 17.3° at 1 second which corresponds to the point of maximum velocity. After 1 second the error decreases until approximately

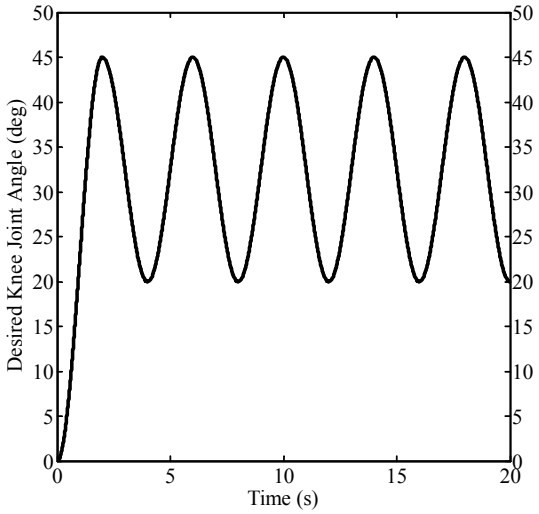

Figure 3–6: Desired tracking profile extended to 20 seconds.

2 seconds when the error reaches steady-state, never exceeding 3.5°. Using three test subjects, a total of eight tracking experiments were performed (the first subject was tested on two separate days). The RMS errors, standard deviation, and steady-state errors for the eight experiments are shown in Table 3–2. The point in time when the system achieved steady-state was estimated to occur at 2 seconds, hence the steady-state errors use data starting at 2 seconds and continuing until the end of the stimulation period.

3.5 Discussion

Results from both experiments were promising. Specifically, the experimental results indicated that with no muscle model (and only voltage amplitude modulation), the RISE algorithm could determine the appropriate stimulation voltage for both regulation and tracking. The RISE algorithm obtained a regulation error of less than 0.5° and a tracking error of approximately 3.5°.

The primary objective of the first experiment was regulating the knee-joint to a desired final angle (45°). The experiment showed a well behaved transient and

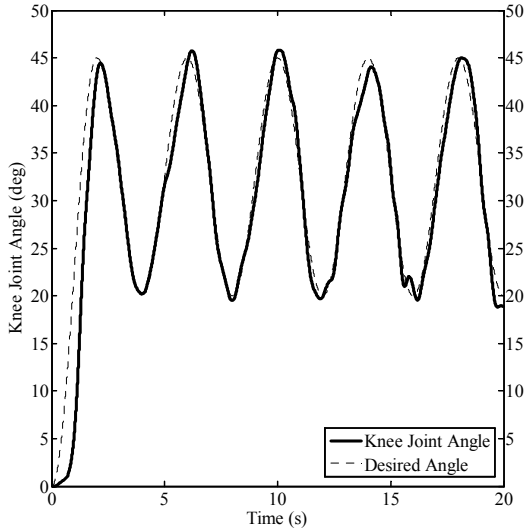

Figure 3–7: Knee joint tracking using the RISE controller.

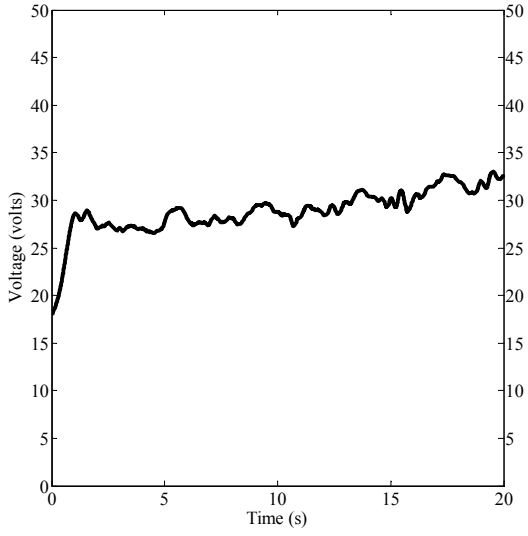

Figure 3–8: Tracking voltage using the RISE controller.

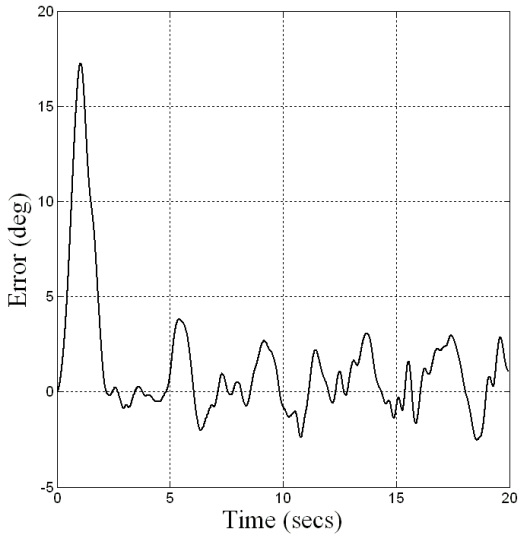

Figure 3–9: Tracking error of knee joint angle (desired angle minus actual angle).

Table 3–2: RMS and steady-state error for RISE tracking experiments

Test Subject	Leg	RMS Error	Steady-state Error (RMS)	Max. Steady-state Error (deg.)	
1	Left	4.383	2.276	8.940	
1	Right	4.621	2.299	7.438	
2	Left	4.193	1.950	5.907	
2	Right	4.721	2.315	6.830	
3	Left	3.561	1.311	3.841	
3	Right	5.362	4.796	5.928	
1	Left	4.701	4.383	4.866	
1	Right	4.751	4.621	5.082	
		4.537	2.994	5.788	Mean
		0.486	1.285	2.097	Standard Deviation

that within three seconds the error was within 4°. After 3.8 seconds the error never exceeded 0.5°.

The objective for the second experiment required the knee-joint to track a desired sinusoidal trajectory with a period of four-seconds. The experiment showed that at the point of maximum velocity (one-second), the controller had a transient error of 17.3°. After approximately 2-seconds (the point where the velocity is zero) the knee-joint tracking error never exceeded 3.5°.

3.6 Concluding Remarks

A RISE nonlinear control algorithm was applied to NMES to elicit non-isometric contractions of the human quadriceps muscle. Two experiments were performed to determine the performance of the RISE control method.

Future efforts will focus on implementing different modulation methods, stimulating for functional tasks, examining fatigue induced by the RISE controller, comparing the RISE control results with other NMES methods, and experimental trials on more volunteers, potentially including persons with neurological disorders.

CHAPTER 4
CONCLUSIONS AND RECOMMENDATIONS

Two nonlinear controllers were implemented for non-isometric experiments that controlled a human knee joint angle via NMES of the quadriceps without the use of a muscle model. The first controller was a numerical iterative extremum seeking routine (Brent's Method) that was implemented for two regulation experiments; the first experiment used voltage modulation for NMES, and the second was a self-test that used frequency modulation. The second controller was an implementation of a recently developed scheme coined RISE (Robust Integral Sign of the Error) that used voltage modulation in a regulation experiment and a sinusoidal tracking experiment. The experimental results from Brent's Method showed that with both modulation schemes it was able to position the knee angle within 0.9° it's 45° objective in five iterations. The results for the RISE controller showed that regulation of the knee angle was accurate to within 0.5° of it's 45° objective. For the sinusoidal tracking experiment the RISE controller maintained a steady-state tracking error of approximately 3.5°.

The results shown by this research indicate that it is possible to perform reasonable NMES tracking and regulation control of the human quadriceps muscle group without using a muscle model. Brent's Method is limited due to it's dependence on the knee joint reaching a relative steady-state condition (which may take five seconds) before performing it's next iterations. The RISE controller was very promising with the regulation experiments. Minor adjustments to the gains showed that it can easily accommodate a variety of test subjects with excellent results. Limitations to the RISE method were apparent during the tracking experiment where it showed sensitivity to gain changes.

Expanding upon Brent's extremum seeking routine does not seem fruitful. A feature and limitation of extremum seeking routines is their iterative nature to converge on a solution. While this iterative behavior works well when time between iterations is not an issue, it severely limits its use for NMES.

The RISE controller's limitation is partially due to time delays which occur between the stimulus and the muscle contraction force with non-isometric NMES. When used outside of the NMES field, adding a neural network (NN) to the RISE controller showed improved behavior as time progressed and the NN updated. The inability to develop a consistent mapping between the NMES parameters and the muscle's contraction force could be investigated with a NN that learns an individuals muscle model by using use linear voltage gradients with isometric and non-isometric NMES.

In addition to future control research with non-isometric NMES, the isometric attachment to the LEM enables the ability to perform unique back-to-back experiments that may show insight into time delay issues as well as cause-and-effect of muscle fatigue. With the ultimate motivation of this research being the rehabilitation and potential improvements in the daily activities for people afflicted with neuromuscular disorders such as stroke or spinal cord injuries, future experiments need to include people within this population segment.

APPENDIX
ELECTRICAL DESIGN AND INTERFACING

A.1 Circuit Design for 100 μsec Wide Pulse

Generating a pulse width of 100 μ sec from a system that has a sampling rate of 1000 Hz required building the custom circuit shown in Figure A–1. After building a prototype of the circuit and verifying its behavior the printed circuit board (PCB) was designed and the necessary files were sent to Imagineering Inc. to be manufactured (Fig. A–2). Upon return of the bare PCB from the manufacturer it was populated (Fig. A–3), and again its behavior was verified, after which, the PCB to PC interfacing cables were built.

A.2 Circuit Description

The output requirements for the PCB were that it deliver a 100 μsec wide pulse at a frequency and voltage dictated by the controller. The stimulation voltage and frequency are between $0 - 150$ volts and $10 - 1000$ Hz respectively. Figure A–4 shows the stimulation pulse shape that is delivered to the test subject.

The output demands for the PCB (Fig. A–1) required six separate DC input voltages as described in Table A–1. Interfacing the PCB with the Servo To Go I/O card (STG) required four STG outputs; two between -10.0 to $+10.0$ volts DC and two between $0.0 - 10.0$ volts DC.

Generating the 100 μsec wide pulse at varying frequencies and voltages was controlled by a voltage-to-frequency converter (VFC) described below. A power op-amp (described below) uses a $0 - 10$ VDC input then outputs a positive square pulse between $1 - 150$ volts which is fed to the electrodes attached to the test subject.

The complete parts used to build the PCB are listed in Table A–2.

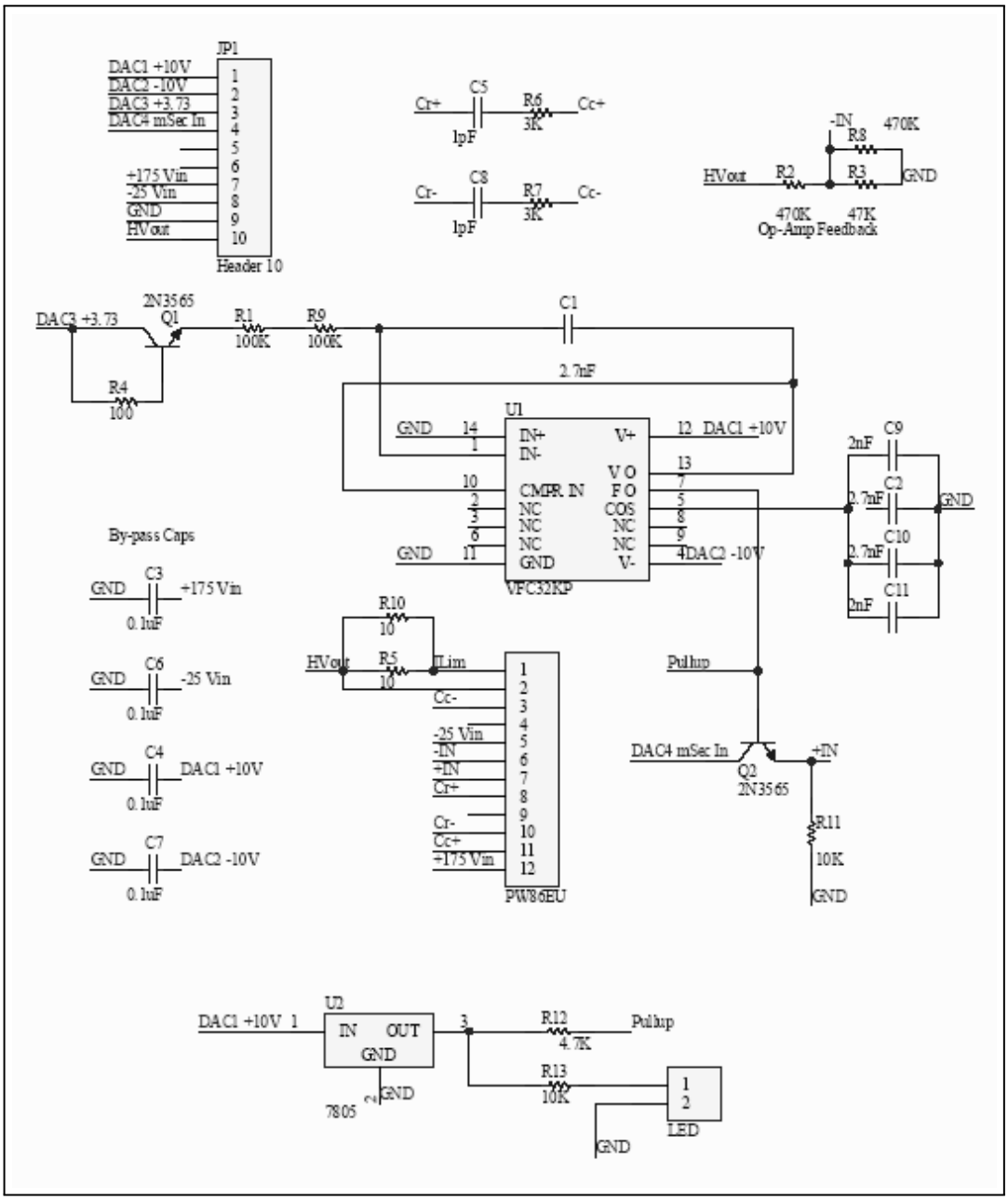

Figure A–1: Schematic of circuitry used to deliver the computed stimulation pulse train.

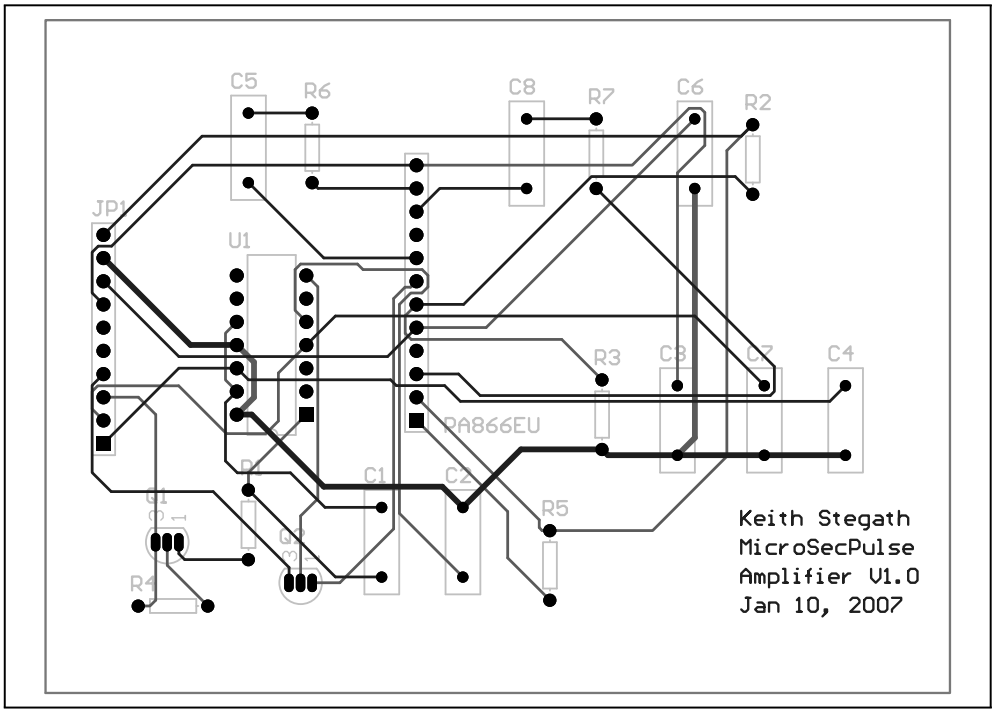

Figure A–2: PCB layout of circuitry used to deliver the computed pulse train.

A.2.1 High Voltage Power Op-Amp PA866EU

The function of the op-amp is to amplify the input signal coming from the STG. The amplified signal (the stimulation voltage computed by the software) is fed directly to the electrodes attached to the test subject's muscles. The op-amp is supplied with three DC voltages. The +175 volts and −25 volts are supplied via a

Table A–1: Input voltages to circuit

DC Signal (volts)	Purpose
+175.0	High voltage input to Op-amp
-25.0	Low voltage input to Op-amp
+10.0	Positive supply voltage for VFC
-10.0	Negative supply voltage for VFC
0.0-10.0	Op-amp control signal for stimulation voltage
0.0-10.0	VFC control signal for stimulation frequency

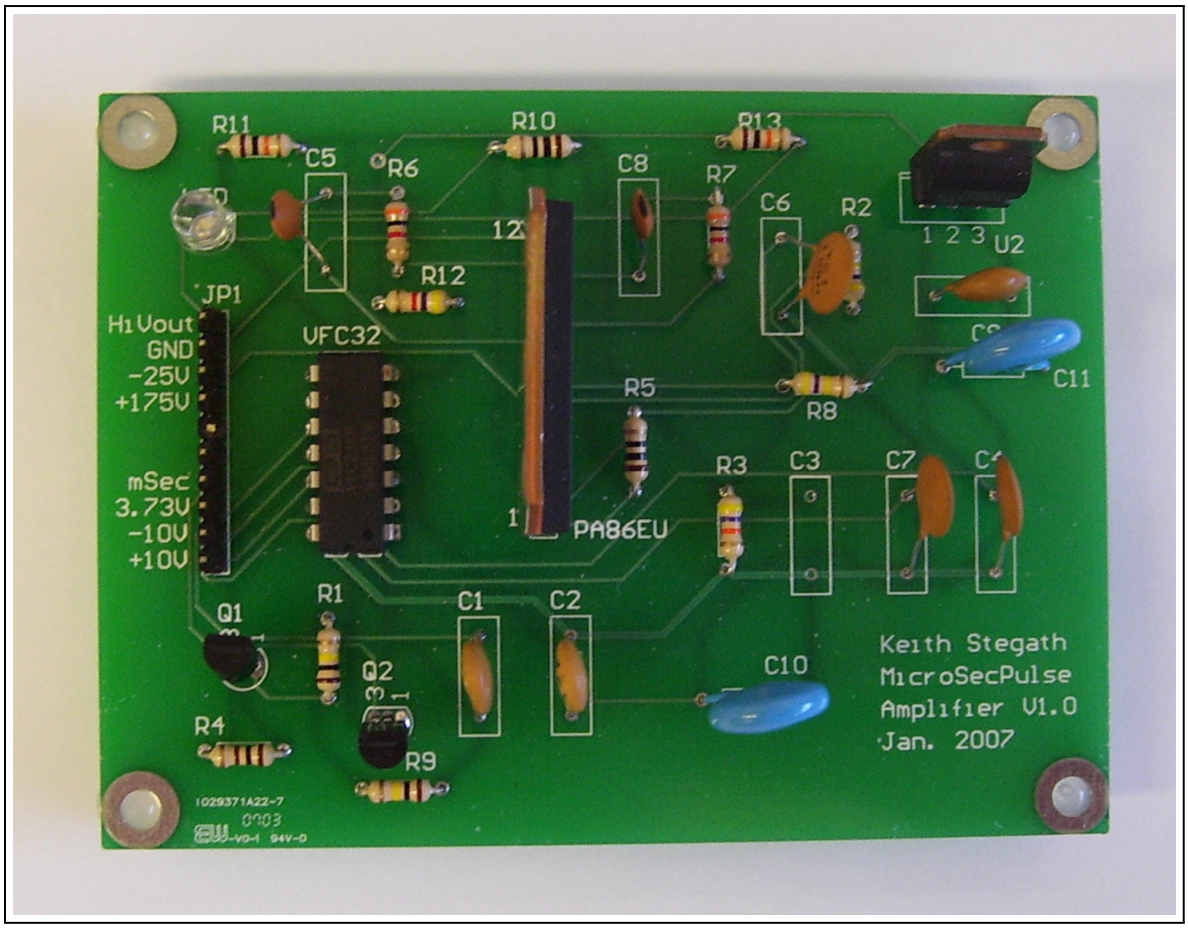

Figure A–3: Circuit board used to generate and amplify a 100 μsec pulse.

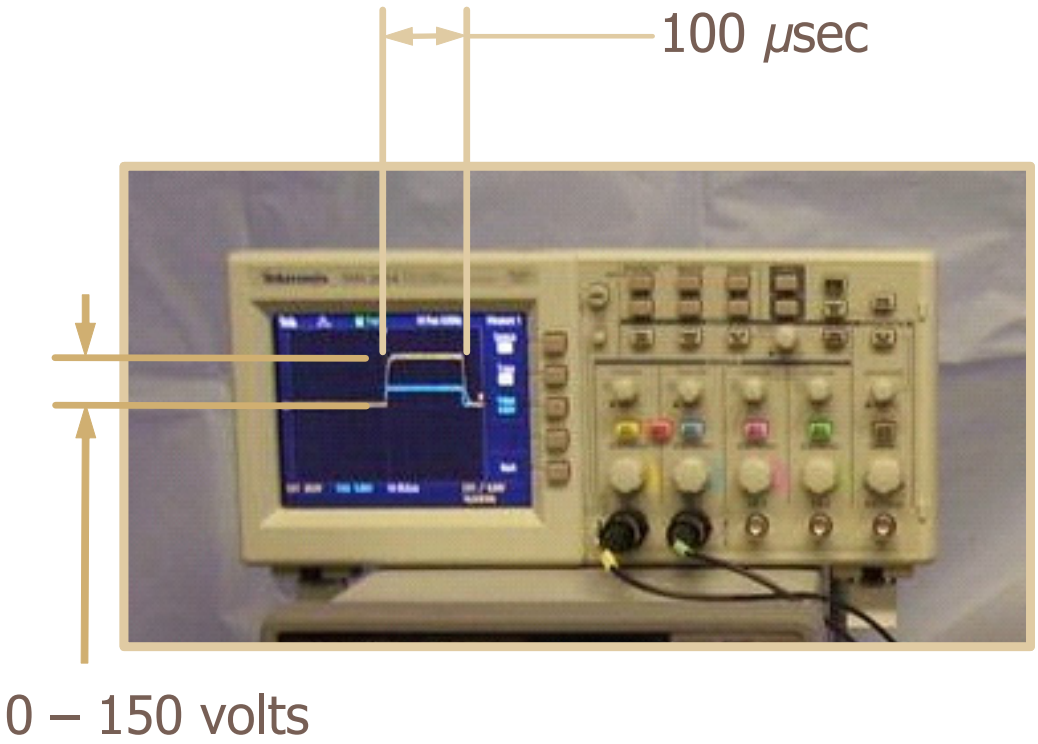

Figure A–4: Shape of stimulation pulse.

commercial power supply and serve to power the op-amp. The third DC signal (0.0 - 10.0 volts) is computed by the software and delivered to the op-amp via the STG. The op-amp is configured as non-inverting with +IN (the voltage to be amplified) being supplied via the emitter of transistor Q2 (Fig. A–1). The negative feedback loop of the op-amp consists of resistors R2 (470kΩ) and R3 (47kΩ), which are configured to give a gain of approximately 10:1. Note: resistor R8 is no longer used.

A.2.2 Voltage to Frequency Conversion - VFC32

Generating the desired stimulation frequency and the 100 μsec wide pulse is controlled by a voltage-to-frequency converter integrated circuit (IC). The VFC is supplied with three DC voltages shown in Table A–1. The −10 volts and +10 volts power the VFC and are supplied via the STG. The third DC signal (0.0 - 10.0 volts) is computed by the software and determines the signal frequency. Generation of the 100 μsec wide pulse is controlled by the proper selection of capacitors and

Table A–2: Parts list for stimulator circuit

Quantity	Part Number	Description
1	APEX PA866EU	High voltage power op-amp
1	Texas Inst. VFC32	Voltage to frequency converter
2	10kΩ Resistor	Current limiter
1	4.7kΩ Resistor	Pull up
2	100kΩ Resistor	R1, R2 - VFC circuit
1	100Ω Resistor	Q1 Bias
2	10Ω Resistor	Op-amp current limiter
2	3kΩ Resistor	Op-amp compensation
1	470kΩ Resistor	Op-amp feedback
1	47kΩ Resistor	Op-amp feedback
3	2.7nF Cap	VFC control
4	0.1μF Cap	Bypass capacitor
2	2nF Cap	VFC control
2	2pF Cap	Op-amp compensation
1	7805	5 volt supply - pull up & LED
1	LED	Stimulation status
2	2N3565	NPN transistor

remains constant throughout the VFC frequency range. The array of parallel capacitors C2, C9-C10 are used by the VFC in order to generate the 100 μsec pulse width. The series resistors R1 & R9 determine the frequency range when supplied a $0 - 10$ VDC output from the STG. The frequency range is $10 - 1000$ Hz. The voltage supplied to pin 1 of the VFC (labeled IN- in Fig A–1), (supplied from the STG) determines the VFC's output frequency.

A.2.3 Transistors 2N3565

Transistors 2N3565 are type NPN and are used in switching mode. Transistor Q1 supplies the DC voltage output from the STG to pin 1 of VFC (labeled IN- in Fig. A–1). The base of transistor Q2 is connected to the output of the VFC. The collector of Q2 is connected to a DC voltage from the STG. The emitter from Q2 is connected to the +IN of the op-amp PA866EU.

A.2.4 Voltage Regulator 7805

The 7805 voltage regulator supplies 5 volt DC power to the LED (which indicates communication with the STG) and as a pull-up supply to the base of transistor Q2 (enabling it to function as a digital switch), and the output of the VFC.

A.2.5 Circuit Behavior

The overall outline of circuit's behavior is as follows:

- The STG supplies a $0 - 10$ VDC signal to IN- of the VFC which determines the frequency.
- The STG supplies a $0 - 10$ VDC signal to collector of Q2 which is the scaled down stimulation voltage.
- The output signal from the VFC is digital (0 or 5 volts) and is fed to the base of Q2. The output signal developed by the VFC contains the frequency ($10 - 100$ Hz), and contained within that signal is the pulse width (100 μsec).
- When the base of Q2 is high it's emitter supplies the scaled-down stimulation voltage to +IN of the op-amp.
- The output of the op-amp carries the entire amplified stimulation signal: The stimulation voltage is delivered to the test subject with a 100 μsec wide pulse that occurs at the desired frequency.

A.3 Interfacing the 100 μsec Wide Pulse PCB to the Computer

Generating the desired frequency and stimulation voltage required correlating the two $0 - 10$ VDC output signals from the STG to the PCB. The correct mapping voltages were obtained empirically by recording two sets of data-pairs. Using a commercial power supply, ten randomly chosen DC voltages were input to the PCB's frequency and stimulation voltage pins. The output from the PCB was observed on an oscilloscope and the corresponding data-pairs were recorded and entered into MATLAB where two polynomials were generated by using the

POLYFIT and POLYVAL routines. The polynomials were then hard-coded into a C++ program. The accuracy of the polynomials was verified by inputting a desired frequency and stimulation voltages while observing the PCB's output on an oscilloscope.

A.4 Circuit Design for Multiples of 25 μsec Wide Pulse

The method that allows the NMES controller to increase or decrease the pulse width in steps of 25 μsec is performed with six relays controlled by two analog multiplexers (MUX). The circuit (Fig. A–5) was developed as a separate add-on circuit board interfaced to the PCB and the STG.

A.4.1 Circuit Description

The output of the circuit is akin to that of a variable capacitor. The output (a capacitance) is placed in parallel with capacitors C2 and C9-C10 on the main PCB. The combined capacitance determines the pulse width generated by the VFC.

Input to the circuit consists of eight digital signals supplied by the STG and a six-volt DC power supply. The eight digital signals control the output of the two MUXes that determine which relays are energized. The relays are configured as two-sets of three and are labelled *Relay 1 Array* (RA1) and *Relay 2 Array* (RA2) as shown in Fig. A–5. The purpose of RA1 is to control the portion of the pulse width which is a multiple of 100 μsec. The purpose of RA2 is to control the portion of the pulse width which is a multiple of 25 μsec. Functioning together, RA1 and RA2 allow for a pulse width of $100 - 675$ μsec.

The functioning of each relay array is identical so the following discussion of RA1 also applies to RA2. RA1 is controlled by the analog multiplexer labeled U2. The multiplexer U2 receives four digital signals from the STG labeled A-I, B-I, C-I, and E-I (Fig. A–5) whose states determine which relay(s) to energize. The signals A-I, B-I, C-I, and E-I are determined by the NMES controller and are based on the desired pulse width. U2 decodes the four digital signals then energizes the

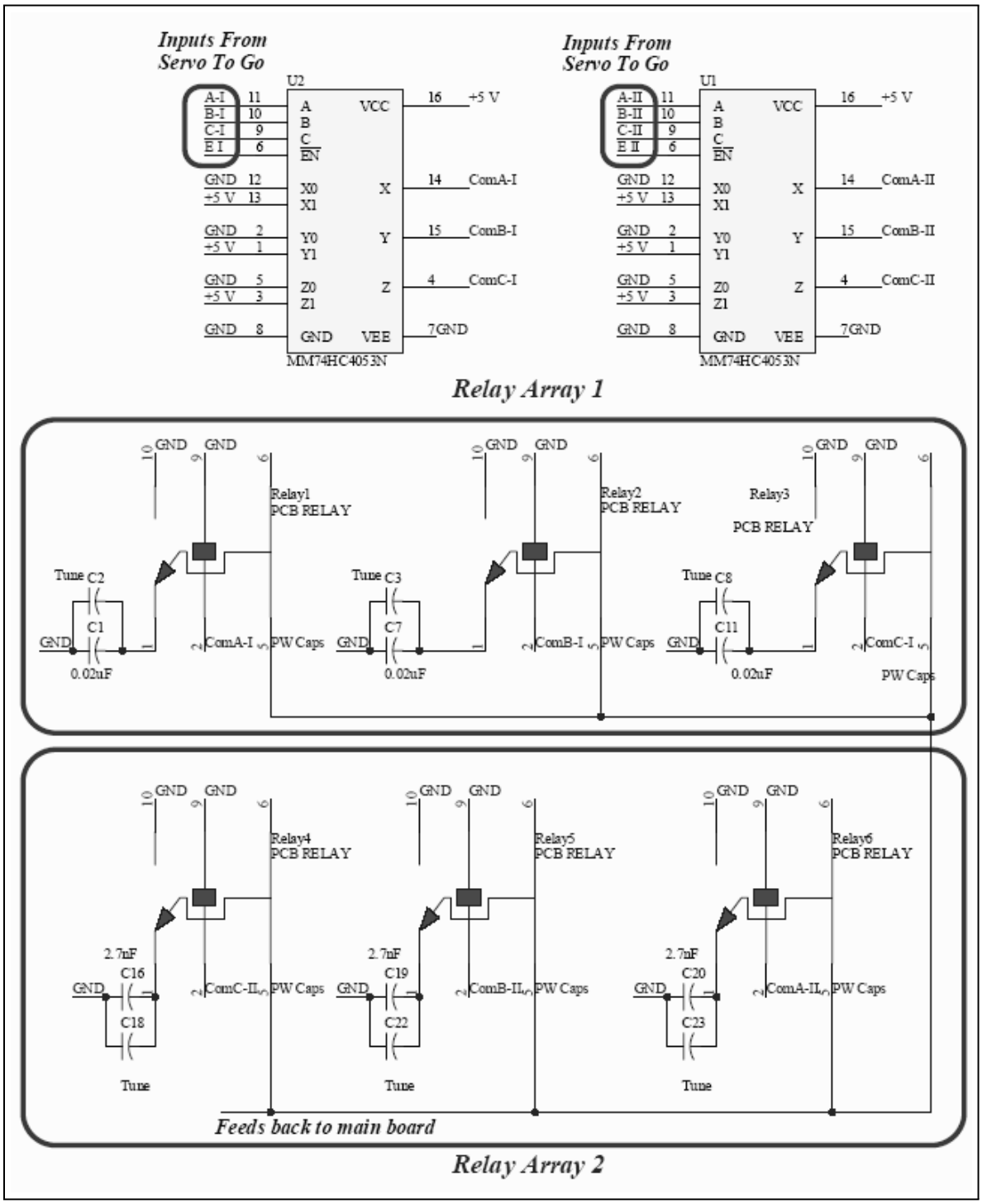

Figure A–5: Circuit for adjusting the pulse width with steps of 25 μsec.

Table A–3: Digital inputs to the circuit

Digital Inputs to 74HC405$\mathbf{3}_{1,2}$ from Servo To Go	Purpose
D_1	A_1 - Relay 1
D_2	B_1 - Relay 1
D_3	C_1 - Relay 1
D_4	E_1 - Relay 1
D_5	A_2 - Relay 2
D_6	B_2 - Relay 2
D_7	C_2 - Relay 2
D_8	E_2 - Relay 2

Table A–4: The effect of the relay on the corresponding pulse width

Relay_{1-6}	Purpose
1	100 μsec step
2	300 μsec step
3	200 μsec step
4	25 μsec step
5	25 μsec step
6	25 μsec step

corresponding relays in RA1. The combined states of the RA1 determine which capacitors are in the circuit, hence the overall capacitance appearing at "*Feeds back to main board*" in Fig. A–5. The capacitance of circuit A–5 is in parallel with capacitors C2 and C9-C10 on the PCB which determines the capacitance seen by the VFC (which determines the pulse width).

Table A–3 shows the STG connections to the MUXes and which relays are used to control their portion of the pulse width. Various combinations of Relays_{1-3} give multiples of 100 μsec pulse width's from 100 - 600 μsec. Relays_{4-6} each add an additional 25 μsec to the pulse width. Table A–4 shows the relay's effect on the pulse width ranging between $100 - 675$ μsec in 25 μsec increments.

The list of parts for the pulse width controller is shown in Table A–5.

Table A–5: Parts list for pulse width controller

Quantity	Part Number	Description
6	Omron G5V-1	5 volt PCB mount relay
2	Fairchild 74HC4053	Analog Multiplex
12	0.10 μF	Capacitor
6	$0.01 - 0.05$ μF	Tuning capacitor

A.5 Isometric Attachment

Isometric experiments are performed by attaching a S-beam load cell (LC) between the swing-arm and the frame of the LEM. The LC is rated for 300 lbs. in tension and compression. Output from the LC is amplified 1000 times by an instrumentation op-amp. The circuit diagram for the LC circuit is shown in Fig. A–6. The input to the LC circuit is ± 10 VDC for load cell excitation. Output from the LC is $0 - 10$ VDC which is monitored by an analog-to-digital input on the STG.

The LC output was calibrated by suspending it then adding known weights to the free end and recording the output voltages. The output was linear, requiring only slope and y-intercept offsets.

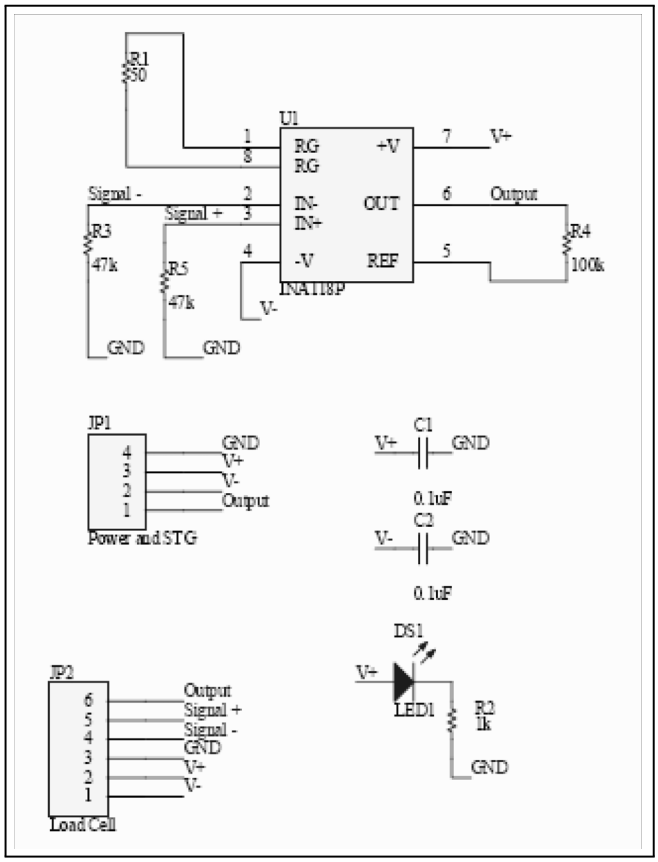

Figure A–6: Circuit diagram for S-beam load cell.

REFERENCES

[1] P. H. Peckham and D. B. Gray, "Functional neuromuscular stimulation," *J. Rehab. Research Dev.*, vol. 33, pp. 9–11, 1996.

[2] J. J. Abbas and H. J. Chizeck, "Feedback control of coronal plane hip angle in paraplegic subjects using functional neuromuscular stimulation," *IEEE Trans. Biomed Eng.*, vol. 38, no. 7, pp. 687–698, 1991.

[3] N. Lan, P. E. Crago, and H. J. Chizeck, "Control of end-point forces of a multijoint limb by functional neuromuscular stimulation," *IEEE Trans. Biomed. Eng.*, vol. 38, no. 10, pp. 953–965, 1991.

[4] ——, "Feedback control methods for task regulation by electrical stimulation of muscles," *IEEE Trans. Biomed. Eng.*, vol. 38, no. 12, pp. 1213–1223, 1991.

[5] T. Schauer, N. O. Negard, F. Previdi, K. J. Hunt, M. H. Fraser, E. Ferchland, and J. Raisch, "Online identification and nonlinear control of the electrically stimulated quadriceps muscle," *Control Engineering Practice*, vol. 13, pp. 1207–1219, 2005.

[6] K. Stegath, N. Sharma, C. M. Gregory, and W. E. Dixon, "An extremum seeking method for non-isometric neuromuscular electrical stimulation," in *IEEE Int. Conf. Syst., Man, Cybern.*, 2007, accepted, to appear.

[7] M. Ferrarin, E. Pavan, R. Spadone, R. Cardini, and C. Frigo, "Standing up exerciser based on functional electrical stimulation and body weight relief," *Medical and Biological Engineering and Computing*, vol. 40, no. 3, pp. 282–289, 2002.

[8] G. Khang and F. E. Zajac, "Paraplegic standing controlled by functional neuromuscular stimulation: Part I - computer model and control-system design," *IEEE Trans. Biomed. Eng.*, vol. 36, no. 9, pp. 873–884, 1989.

[9] F. Previdi, M. Ferrarin, S. Savaresi, and S. Bittanti, "Gain scheduling control of functional electrical stimulation for assisted standing up and sitting down in paraplegia: a simulation study," *International Journal of Adaptive and Signal Processing*, vol. 19, pp. 327–338, 2005.

[10] H. Kordylewski and D. Graupe, "Control of neuromuscular stimulation for ambulation by complete paraplegics via artificial neural networks," *Neurol Res.*, vol. 23, no. 5, pp. 472–481, 2001.

[11] J. A. Riess and J. J. Abbas, "Adaptive neural network control of cyclic movements using functional neuromuscular stimulation," *IEEE Trans. Rehab. Eng.*, vol. 8, pp. 42–52, 2000.

[12] E. C. Stites and J. J. Abbas, "Sensitivity and versatility of an adaptive system for controlling cyclic movements using functional neuromuscular stimulation," *IEEE Trans. Biomed. Eng.*, vol. 47, pp. 1287–1292, 2000.

[13] K. Y. Tong and M. H. Granat, "Gait-control system for functional electrical stimulation using neural networks," *Med. Bio. Eng. Comput.*, vol. 37, pp. 35–41, 1999.

[14] F. Sepulveda, M. H. Granat, and A. Cliquet, "Two artificial neural systems for generation of gait swing by means of neuromuscular electrical stimulation," *Med. Eng. Phys.*, vol. 19, pp. 21–28, 1997.

[15] F. Sepulveda, *Computer Techniques in Medical and Biotechnology Systems*. Kluwer Academic Pub., Amsterdam, 2003.

[16] D. G. Zhang and K. Y. Zhu, "Simulation study of fes-assisted standing up with neural network control," in *IEMBS 26th Annual International IEEE Conf. Engineering in Medicine and Biology Society*, vol. 6, 2004, pp. 4118–4121.

[17] J. P. Giuffrida and P. E. Crago, "Functional restoration of elbow extension after spinal-cord injury using a neural network-based synergistic fes controller," *IEEE Trans. Neural Syst. Rehabil. Eng.*, vol. 13, no. 2, pp. 147–152, 2005.

[18] Y. Chen, W. Chen, C. Hsiao, T. Kuo, and J. Lai, "Development of the fes system with neural network + PID controller for the stroke," in *IEEE International Symposium on Circuits and Systems*, vol. 5, 2005, pp. 5119–5121.

[19] P. F. Blackman, *An Exposition of Adaptive Control*. Macmillan, 1962, ch. Extremum-seeking regulators, pp. 36–50.

[20] O. L. R. Jacobs and G. C. Shering, "Design of a single-input sinusoidal perturbation extremum-control system," *Proc. Inst. Elect. Eng.*, vol. 115, pp. 212–217, 1968.

[21] V. V. Kazakevich, "Extremum control of objects with inertia and of unstable objects," *Sov. Phys. J.*, pp. 658–661, 1960.

[22] I. S. Morosanov, "Method of extremum control„" *Automat. Remote Contr.*, vol. 18, pp. 1077–1092, 1957.

[23] I. I. Ostrovskii, "Extremum regulation," *Automat. Remote Contr.*, vol. 18, pp. 900–907, 1957.

[24] B. Kartik and M. Krstic, *Real-Time Optimization by Extremum Seeking Feedback*. Hoboken, New Jersey: Wiley, 2003.

[25] G. M. Graham, T. A. Thrasher, and M. R. Popovic, "The effect of random modulation of functional electrical stimulation parameters on muscle fatigue," *IEEE Trans. Neural Syst. Rehabil. Eng.*, vol. 14, no. 1, pp. 38–45, 2006.

[26] C. M. Gregory, W. E. Dixon, and C. S. Bickel, "Impact of varying pulse frequency and duration on muscle function during nmes," *Muscle and Nerve*, vol. 35, no. 4, pp. 504–509, 2007.

[27] P. M. Patre, W. MacKunis, C. Makkar, and W. E. Dixon, "Asymptotic tracking for systems with structured and unstructured uncertainties," *IEEE Trans. Contr. Syst. Technol.*, 2006, accepted, to appear.

[28] ——, "Asymptotic tracking for systems with structured and unstructured uncertainties," in *IEEE Conference on Decision and Control*, 2006, pp. 441–446.

[29] W. H. Press, S. A. Teukosky, W. T. Vetterly, and B. P. Flamneny, *Numerical Recipes in Fortran, the Art of Scientific Computing*, 2nd ed. Cambridge University Press, 1992.

[30] M. Krstic and H. Deng, *Stabilization of Nonlinear Uncertain System*. Springer-Verlag, 1998.

[31] X. T. Zhang, D. M. Dawson, W. E. Dixon, and B. Xian, "Extremum seeking nonlinear controllers for a human exercise machine," *IEEE Transactions on Mechatronics*, vol. 11, no. 2, pp. 233–240, 2006.

[32] M. Loffler, N. Costescu, and D. Dawson, "Qmotor 3.0 and the qmotor robotic toolkit - an advanced pc-based real-time control platform," *IEEE Control Syst. Mag.*, vol. 22, no. 3, pp. 12–26, 2002.

[33] M. Ferrarin and A. Pedotti, "The relationship between electrical stimulus and joint torque: [a] dynamic model," *IEEE Trans. Rehabil. Eng.*, vol. 8, no. 3, pp. 342–352, 2000.

[34] J. L. Krevolin, M. G. Pandy, and J. C. Pearce, "Moment arm of the patellar tendon in the human knee," *Journal of Biomechanics*, vol. 37, pp. 785–788, 2004.

[35] W. L. Buford, Jr., F. M. Ivey, Jr., J. D. Malone, R. M. Patterson, G. L. Peare, D. K. Nguyen, and A. A. Stewart, "Muscle balance at the knee - moment arms for the normal knee and the acl - minus knee," *IEEE Trans. Rehabil. Eng*, vol. 5, no. 4, 1997.

[36] V. I. Utkin, *Sliding Modes in Control and Optimization*. New Yord: Springer-Verlag, 1992.

[37] B. Xian, D. M. Dawson, M. S. de Queiroz, and J. Chen, "A continuous asymptotic tracking control strategy for uncertain multi-input nonlinear systems," *IEEE Trans. Autom. Control*, vol. 49, no. 7, pp. 1206–1211, 2004.

[38] C. Makkar, G. Hu, W. G. Sawyer, and W. E. Dixon, "Lyapunov-based tracking control in the presence of uncertain nonlinear parameterizable friction," *IEEE Trans. Autom. Control*, 2007, accepted, to appear Oct. 2007.

BIOGRAPHICAL SKETCH

Keith Stegath was born in Ann Arbor, Michigan. In 2005, he received a Bachelor of Science degree in electrical engineering from the University of Florida. In 2002, he received an Associate of Arts degree from SantaFe Community College, in Gainesville, Florida. While attending Ferris State University in Big Rapids, Michigan, from 1975 to 1978, he received an Associate of Science degree in automotive technology and a machinist certificate.

From 1993 to 1999, he was sole proprietor of Stegath Coachcraft which performed complete restorations on classic automobiles. He was a software engineer with Applicon CAD/CAM from 1988 to 1993. From 1986 to 1988, he was the sole proprietor of CADsultants where he worked with the CAD/CAM industry and developed a custom automobile based on the Corvette chassis. From 1986 to 1987, he was a CAD/CAM Coordinator with Troy Design where he developed a procedure for generating CNC tool paths from a CAD solid model database. From 1980 to 1986, he was an Application and Product Engineer at Manufacturing Data System Inc. where he provided technical support for customers using computer assisted programming of their CNC machines. From 1978 to 1980, he was a machinist. He worked at Jasper Auto Parts and Machine Shop machining and rebuilding automobile engines, then at Electro Arc Manufacturing setting up manual mills and lathes and manual programming a CNC mill. For a short period of time he was an automechanic at Long Chevrolet.

From 1998 to 2000, he wrote science fiction techno-thrillers. He wrote six short stories, completed one novel, and in 2000 worked with a published author on a second novel.